1

Comprehensive preclinical evaluation of human-derived anti-poly-GA antibodies in cellular and animal models of C9ORF72 disease

Melanie Jambeau[1,2,3,#], Kevin D. Meyer[4,8,#], Marian Hruska-Plochan[3,#], Ricardos Tabet[1,2], Chao-Zong Lee[1,2], Ananya Ray-Soni[1,2], Corey Aguilar[1,2], Kitty Savage[1,2], Nibha Mishra[1,2], Nicole Cavegn[4], Petra Borter[4], Chun-Chia Lin[1], Karen Jansen-West[5], Jay Jiang[6], Fernande Freyermuth[1,2], Nan Li[1,2], Pierre De Rossi[3], Manuela Pérez-Berlanga[3], Xin Jiang[1,2], Lilian M. Daughrity[5], Joao Pereira[1,2], Sarav Narayanan[7], Yuanzheng Gu[7], Shekhar Dhokai[7], Isin Dalkilic-Liddle[7], Zuzanna Maniecka[3], Julien Weber[3], Michael Workman[1], Melissa McAlonis-Downes[6], Eugene Berezovski[1,2], Yong-Jie Zhang[5], James Berry[1], Brian J. Wainger[1,2], Mark W. Kankel[7], Mia Rushe[7], Christoph Hock[4,8], Roger M. Nitsch[4,8], Don W. Cleveland[6], Leonard Petrucelli[5], Tania Gendron[5], Fabio Montrasio[4], Jan Grimm[4,*], Magdalini Polymenidou[3,*], Clotilde Lagier-Tourenne[1,2,*]

[1] Department of Neurology, The Sean M. Healey and AMG Center for ALS at Mass General, Massachusetts General Hospital and Harvard Medical School, Boston, MA 02114, USA.

[2] Broad Institute of Harvard and MIT, Cambridge, MA 02142, USA.

[3] Department of Quantitative Biomedicine, University of Zurich, Winterthurerstrasse 190, CH-8057 Zurich, Switzerland.

[4] Neurimmune AG, Wagistrasse 18, CH-8952 Schlieren, Switzerland.

[5] Department of Neuroscience, Mayo Clinic, Jacksonville, FL 32224, USA.

[6] Ludwig Institute for Cancer Research, University of California San Diego, La Jolla, CA 92093.

[7] Biogen, Cambridge, Massachusetts, 02142, USA.

[8] Institute for Regenerative Medicine, University of Zurich, Wagistrasse 12, CH-8952 Schlieren, Switzerland.

[#] These authors contributed equally.

[*] Corresponding authors

Emails for correspondence: jan.grimm@neurimmune.com or

magdalini.polymenidou@uzh.ch or clagier-tourenne@mgh.harvard.edu

Abstract

Hexanucleotide G_4C_2 repeat expansions in the *C9ORF72* gene are the most common genetic cause of amyotrophic lateral sclerosis (ALS) and frontotemporal dementia (FTD). Dipeptide repeat proteins (DPRs) generated by translation of repeat-containing RNAs show toxic effects *in vivo* as well as *in vitro* and are key targets for therapeutic intervention. We generated human antibodies that bind DPRs with high affinity and specificity. Anti-GA antibodies engaged extra- and intracellular poly-GA and reduced aggregate formation in a poly-GA over-expressing human cell line. However, antibody treatment in human neuronal cultures synthesizing exogenous poly-GA resulted in the formation of large extracellular immune complexes and did not affect accumulation of intracellular poly-GA aggregates. Treatment with antibodies was also shown to directly alter the morphological and biochemical properties of poly-GA and to shift poly-GA/antibody complexes to more rapidly sedimenting ones. These alterations were not observed with poly-GP and have important implications for accurate measurement of poly-GA levels including the need to evaluate all centrifugation fractions and disrupt the interaction between treatment antibodies and poly-GA by denaturation. Targeting poly-GA and poly-GP in two mouse models expressing G_4C_2 repeats by systemic antibody delivery for up to 16 months was well-tolerated and led to measurable brain penetration of antibodies. Long term treatment with anti-GA antibodies produced improvement in an open field movement test in aged C9ORF72[450] mice. However, chronic administration of anti-GA antibodies in AAV-$(G_4C_2)_{149}$ mice was associated with increased levels of poly-GA detected by immunoassay and did not significantly reduce poly-GA aggregates or alleviate disease progression in this model.

57

Significance

Immunotherapy has been proposed for neurodegenerative disorders including Alzheimer's or Parkinson's diseases. Recent reports using antibodies against poly-GA or active immunization suggested similar immunotherapy in ALS/FTD caused by repeat expansion in the C9ORF72 gene (1, 2). Here, we systematically characterized human antibodies against multiple DPR species and tested the biological effects of antibodies targeting poly-GA in different cellular and mouse models. Target engagement was shown in three independent cellular models. Anti-GA antibodies reduced the number of intracellular poly-GA aggregates in human T98G cells but not in cultured human neurons. Whereas chronic anti-GA treatment in BAC C9ORF72^{450} mice did not impact poly-GA levels and modestly improved one behavioral phenotype, poly-GA levels detected by immunoassays were increased and disease progression was unaltered in AAV-$(G_4C_2)_{149}$ mice.

70

71

Introduction

73 Hexanucleotide repeat expansions (G_4C_2) in the *C9ORF72* gene are the most frequent genetic

74 cause of amyotrophic lateral sclerosis (ALS) and frontotemporal dementia (FTD) (3, 4).

75 Proposed disease mechanisms include *C9ORF72* haploinsufficiency, repeat-RNA toxicity

76 and protein toxicity. Though the relative contribution of each mechanism is not fully

77 understood (5), there is mounting evidence that accumulation of dipeptide repeat proteins

78 (DPRs), generated by repeat-associated non-ATG (RAN) translation across the *C9ORF72*

79 expansion, plays a crucial role in neurodegeneration (6-11). DPRs are translated from both

80 sense (poly-GA, poly-GR and poly-GP) and antisense (poly-PR, poly-PA and poly-GP)

81 repeat-containing RNAs, and represent the major component of p62-positive, TDP-43-

82 negative aggregates in the central nervous system of C9ORF72 ALS/FTD patients (12-14).

83 Moreover, several *in vivo* and *in vitro* studies support direct toxic effects of arginine-rich

84 DPR proteins poly-PR and poly-GR (15-19), as well as the aggregation-prone and most

85 abundant DPR product, poly-GA (20-22). A recent study directly comparing congenic mice

86 expressing either poly-GA or poly-PR indicates that poly-GA is considerably more toxic,

87 leading to TDP-43 abnormalities and neuronal loss (23), highlighting its suitability as a

88 therapeutic target.

89 Passive immunotherapy using humanized or fully human antibodies targeting aberrantly

90 produced or misfolded proteins has been investigated in several pre-clinical and clinical

91 settings for the treatment of neurodegenerative disorders (24, 25). The most advanced

92 programs have targeted extracellular amyloid-β plaques in mouse models and patients with

93 Alzheimer's disease (26, 27). Targeting intracellular misfolded proteins, including tau and α-

94 synuclein, has also shown beneficial effects on pathology and behavioral abnormalities in

95 multiple mouse models of Alzheimer's (28, 29) or Parkinson's diseases (30). Recently,

96 human-derived antibodies targeting misfolded SOD1 were reported to delay disease onset

4

97   and increase survival in independent ALS-linked SOD1 mutant mouse models (31). Another

98   study explored the potential of immunotherapy for treating C9ORF72 ALS/FTD by using a

99   mouse-derived antibody against poly-GA in cultured cells (32), and a potential beneficial

100   effect of poly-GA human-derived antibodies was reported in C9ORF72 BAC transgenic mice

101   expressing 500 repeats (1). Most recently, the effect of active immunization against poly-GA

102   (2) was assessed in a mouse model overexpressing poly-GA fused with the cyan fluorescent

103   protein ($(GA)_{149}$-CFP;). Reduction in poly-GA accumulation, neuroinflammation and TDP-

104   43 mislocalization was observed in $(GA)_{149}$-CFP mice immunized with ovalbumin-$(GA)_{10}$

105   conjugates (2). Several non-exclusive mechanisms have been proposed for antibody-

106   mediated neutralization of intra-cellular aggregates. In particular, antibodies to tau or α-

107   synuclein may influence disease progression by inhibiting cell-to-cell propagation of toxic

108   proteins (29, 33), a mechanism proposed also for C9ORF72 DPRs (22, 32, 34). Moreover,

109   several studies suggest that antibodies are internalized by neuronal cells (35, 36), where they

110   may capture accumulated protein aggregates and facilitate their degradation.

111   Here, we systematically characterized 11 human anti-DPR antibodies generated by immune

112   repertoire analyses of healthy elderly donors, and tested poly-GA antibodies in multiple cell

113   lines, including human neuronal cultures and two C9ORF72 mouse models. Poly-GA-

114   specific antibodies entered cultured neurons and colocalized with their target in intracellular

115   vesicles. Moreover, long-term antibody treatment of human neurons expressing poly-GA

116   resulted in capturing of extracellular poly-GA and lead to the formation of extracellular

117   antibody-poly-GA complexes. In transgenic mice expressing the *C9ORF72* gene containing

118   450 G_4C_2 repeats ($C9^{450}$) or in mice expressing 149 G_4C_2 repeats within the central nervous

119   system by means of adeno-associated virus (AAV-G_4C_2) (37, 38), antibodies were shown to

120   cross the blood-brain barrier without obvious adverse effects upon long term chronic

121   administration. However, in the $(AAV-G_4C_2)_{149}$ mice antibody treatment was not efficient in

122   clearing poly-GA aggregates and was associated with increased poly-GA levels measured by

123   immunoassay. While an improvement was observed in one behavioral assay in $C9^{450}$ mice,

124   treatment was not associated with alleviation of disease progression in $(AAV-G_4C_2)_{149}$ mice.

125   **Results**

126   **Antibody generation and affinity determination**

127   Human monoclonal antibodies targeting the five *C9ORF72* DPRs were generated by

128   screening memory B-cell libraries from healthy elderly subjects, an approach previously used

129   to identify potent antibodies recognizing protein aggregates that include amyloid-β, SOD1 or

130   α-synuclein (25). Eleven antibodies with high affinity to one or multiple DPRs were

131   characterized by ELISA (*SI Appendix,* **Table S1**, **Fig. S1***A*), biolayer interferometry (*SI*

132   *Appendix,* **Table S1**, **Fig. S1***B*) and immunostaining (*SI Appendix,* **Table S1**, **Fig. S2-6**).

133   Four poly-GA-specific antibodies, designated α-GA$_{1-4}$, were identified with nanomolar EC$_{50}$

134   constants (0.2-0.3 nM) (*SI Appendix,* **Table S1**, **Fig. S1***A*). Kinetic analyses by biolayer

135   interferometry revealed that the four α-GA antibodies had comparable association rate

136   constants (k_a) to GA$_{15}$ peptides. α-GA$_{2-4}$ showed comparably low dissociation rates (k_d),

137   whereas faster target dissociation was observed for α-GA$_1$ (*SI Appendix*, **Table S1**, **Fig. S1***B*).

138   Antibody α-GP$_1$ displayed high affinity binding to poly-GP and a 26-fold lower affinity to

139   poly-GA (*SI Appendix*, **Table S1**, **Fig. S1***A*). By screening against the arginine-rich DPR

140   proteins, poly-GR and poly-PR, we further identified α-PR$_2$, which exclusively recognized

141   poly-PR (EC$_{50}$ of 12.8 nM), as well as several antibody candidates targeting more than one

142   DPR species, α-PR$_{1,3}$ and α-GR$_1$. Two candidates with high affinity EC$_{50}$ binding (0.1-0.4

143   nM) to poly-PA were identified, with α-PA$_1$ specifically targeting poly-PA (*SI Appendix,*

144   **Table S1, Fig. S1***A*).

145   The four human anti-GA (α-GA$_{1-4}$) and the anti-GP (α-GP$_1$) antibodies specifically

146   recognized aggregates in human brain tissues from ALS patients carrying pathogenic

147 expansions in the *C9ORF72* gene (*SI Appendix,* **Table S1**, **Fig. S2A** and *B*, upper panels) and

148 in transgenic mice expressing 450 *C9ORF72* hexanucleotide repeats (C9^{450}) (37) (*SI*

149 *Appendix,* **Table S1, Fig. S2A** and *B*, lower panels). Antibodies targeting poly-GR, poly-PR

150 and poly-PA (α-GR$_1$, α-PR$_{1-3}$ and α-PA$_{1,2}$) failed to detect DPR aggregates following

151 immunostaining of formalin-fixed human and mouse tissues (*SI Appendix,* **Table S1**).

152 To further test antibody specificity across all five DPRs, we transiently transfected motor

153 neuron-like cells (NSC-34) with single DPR species with 50 repeats and tagged with the

154 enhanced green fluorescent protein (GFP) (*SI Appendix,* **Fig. S2-6**). Immunofluorescence

155 analysis revealed a predominantly cytoplasmic, diffuse distribution of GA$_{50}$-GFP, GP$_{47}$-GFP

156 and PA$_{50}$-GFP, with GA$_{50}$-GFP also forming dense and bright aggregates. GR$_{50}$-GFP

157 accumulated either in the cytoplasm or in the nucleus and PR$_{50}$-GFP localized in nuclei. All

158 four human-derived α-GA antibodies (α-GA$_{1-4}$) specifically recognized poly-GA, with no

159 cross-reactivity to other DPR species (*SI Appendix,* **Table S1, Fig. S2** *C* and *D*, **Fig. S3**).

160 Specificity of the α-GA antibodies was confirmed by absence of signal in GFP-only

161 transfected cells and in cells stained with secondary antibody only (*SI Appendix,* **Fig. S4A**).

162 In addition to displaying a strong, specific staining for poly-GP, antibody α-GP$_1$ also showed

163 a weak reactivity for poly-GA, consistent with its *in vitro* binding affinity (EC$_{50}$ values in *SI*

164 *Appendix,* **Table S1**), as well as a faint non-specific nuclear staining (*SI Appendix,* **Fig. S4B**).

165 Two α-PA antibodies, α-PA$_{1,2}$, specifically recognized poly-PA (*SI Appendix,* **Table S1, Fig.**

166 **S5**), while antibodies α-PR$_{2,3}$ detected poly-PR in the nucleus, particularly in nucleoli, but no

167 other DPR species (*SI Appendix,* **Table S1**, **Fig. S6**). Since α-GA and α-GP reliably detected

168 aggregates in C9^{450} mouse and *C9ORF72* ALS patient brain sections, we selected α-GA$_1$, α-

169 GA$_3$ and α-GP$_1$ (or murine chimeric IgG2a derivatives of each: $^{ch}\alpha$-GA$_1$, $^{ch}\alpha$-GA$_3$ and $^{ch}\alpha$-

170 GP$_1$) to test their ability to impact poly-GA and poly-GP accumulation *in vitro* and *in vivo*.

Antibody uptake and colocalization with poly-GA in living cells

To determine if living cells internalize anti-GA antibodies, human neuroblastoma SH-SY5Y cells were transfected to express either a GFP control construct or GA_{50}-GFP and incubated in media containing antibodies α-GA_1, α-GA_3 or an IgG isotype control (50 nM, 72 hrs). A strong antibody signal was detected in SH-SY5Y cells expressing GA_{50}-GFP and treated with α-GA_1 or α-GA_3 compared to cells incubated with an IgG isotype control or cells expressing GFP only (**Fig. 1*A* and *B***, *SI Appendix,* **Fig. S7 *A* and *B***). This result is consistent with the presence of poly-GA within cells enhancing retention of internalized α-GA human antibodies. Automated quantification confirmed colocalization between GA_{50}-GFP and α-GA antibodies. Indeed, 43 % and 55 % of GA_{50}-GFP area colocalized with α-GA_1 and α-GA_3, respectively, while less than 2 % of the GFP-positive area colocalized with these antibodies ($p < 0.001$; **Fig. 1*B***). Importantly, GA_{50}-GFP did not colocalize with the IgG isotype control ($p < 0.001$; **Fig. 1*B***). Similar results were obtained when quantifying the total area of antibodies that colocalized with GFP versus GA_{50}-GFP, with approximately 40 % of the α-GA_1 and α-GA_3 signal overlapping with GA_{50}-GFP, while less than 8 % overlapped with GFP ($p < 0.001$; *SI Appendix,* **Fig. S7*B***).

A flow cytometry-based approach using directly labeled human antibodies (**Fig. 1C**) was used to quantify antibody uptake by SH-SY5Y cells transfected to express HA-GA_{50} or exposed to transfection reagents without any plasmid (mock transfected). After incubation with fluorescently labeled α-GA_1, α-GA_3 or IgG isotype for 24 or 48 hrs, cells were treated with trypsin and trypan blue before analysis by flow cytometry to ensure that the detected fluorescence corresponds to internalized antibodies (36) (**Fig. 1 *C-E*** and *SI Appendix,* **Fig. S7*C-E***). As seen before with confocal microscopy (**Fig. 1*A* and *B*** and *SI Appendix,* **Fig. S7 *A* and *B***), accumulation of poly-GA increased the intracellular α-GA_1 and α-GA_3 antibody signal within 24 (*SI Appendix,* **Fig. S7*C***) or 48 hrs (**Fig. 1 *D* and *E***) compared to cells not

8

196   expressing poly-GA ($p < 0.001$; **Fig 1***E* and *SI Appendix,* **Fig. S7C-E**). Only 2-6 % of the

197   mock transfected (**Fig. 1***E***,** *SI Appendix,* **Fig. S7C**) or the non-transfected cells (*SI Appendix,*

198   **Fig. S7 ***D* and *E*) had detectable internalized antibodies while 15 to 22 % of poly-GA-

199   transfected cells had internalized α-GA$_1$ and α-GA$_3$ antibodies. Notably, internalization of α-

200   GA$_3$ was more efficient than α-GA$_1$ with a trend already observed after 24 hrs of treatment (p

201    $= 0.055$; *SI Appendix,* **Fig. S7C**) and a significant difference after 48 hrs ($p < 0.001$; **Fig. 1***E*).

202   Detectable levels of internalized IgG isotype control were found in less than 9 % of the cells

203   in all conditions.

204   To corroborate these findings, we used an independent, stable and inducible T98G

205   glioblastoma cellular model overexpressing GA$_{161}$-GFP. Following treatment with 100 nM α-

206   GA$_1$ or an IgG isotype control antibody for 72 hrs, cells were stained with anti-human IgG.

207   Image analysis demonstrated that α-GA$_1$ colocalized with poly-GA aggregates within T98G

208   cells, while isotype control was not observed within cells (**Fig. 1***F*). Treatment of T98G cells

209   with α-GA$_1$ reduced the number of aggregates per cell by 29 % (**Fig. 1***G*) and reduced the

210   volume of poly-GA aggregates per cell by 39 % (**Fig. 1***H*).

211   **Antibody uptake and colocalization with poly-GA in human neurons**

212   The enhancement of antibody internalization or retention in presence of poly-GA was also

213   seen in cultured human neurons. Neural stem cells (NSCs) were differentiated for 6 weeks

214   into a functional neural network containing neurons and astrocytes (39), and treated for

215   72 hrs with ^{ch}α-GA$_3$ added to the medium. High-magnification confocal images revealed that

216   ^{ch}α-GA$_3$ was internalized by human neurons (*SI Appendix,* **Fig. S8***A*, upper panels,

217   arrowheads and inset) with no detectable signal in non-treated cells (*SI Appendix,* **Fig. S8***A*,

218   lower panels). Neurons were transduced with a lentivirus expressing doxycycline-inducible

219   GA$_{50}$-GFP and treated for 24 hrs with ^{ch}α-GA$_1$, ^{ch}α-GA$_3$ or an IgG isotype control (**Fig. 2A**

220   and *SI Appendix,* **Fig. S8***B*). Both ^{ch}α-GA$_3$ and the control antibodies were detected as

221   extracellular clumps and internalized by GA_{50}-GFP-expressing neurons at 72 hrs of

222   treatment. While intracellular localization of $^{ch}\alpha$-GA_3 was observed in almost 100 % of GA_{50}-

223   GFP-expressing cells, the IgG isotype control antibody was rarely found accumulated

224   intracellularly (18 %, p < 0.0001; **Fig. 2 *A*** and ***B***). In contrast with $^{ch}\alpha$-GA_3, intracellular $^{ch}\alpha$-

225   GA_1 was detected only after 21 days of treatment (*SI Appendix*, **Fig. S8*B***). Three-dimensional

226   reconstitution of confocal images of GA_{50}-GFP-expressing human neurons treated with $^{ch}\alpha$-

227   GA_3 revealed partial co-localization of GA_{50}-GFP and $^{ch}\alpha$-GA_3 (*SI Appendix*, **Fig. S8*C***).

228   Notably, we observed an incomplete colocalization of $^{ch}\alpha$-GA antibodies with large round

229   intracellular aggregates (*SI Appendix,* **Fig. S8*B***, inset), suggesting that the antibodies may not

230   penetrate the dense core of these structures.

231   To understand the intracellular compartment of the observed antibody-antigen interaction, we

232   performed co-immunostaining of GA_{50}-GFP, $^{ch}\alpha$-GA_3, and either RAB7 (endosomes) or

233   LAMP1 (lysosomes). This analysis revealed that GA_{50}-GFP and antibody partially

234   colocalized with each of these markers (**Fig. 2*C***), supporting that intracellular interaction

235   between poly-GA and externally delivered antibodies occurred within trafficking vesicles. Of

236   note, the presence of the α-GA antibody was not required for the localization of GA_{50}-GFP

237   into endosomal vesicles (**Fig. 2*C***, lower panel). To determine if the presence of intracellular

238   antibody facilitated the engulfment of GA_{50}-GFP in intracellular vesicles, we quantified the

239   colocalization between approximately 1400 GA_{50}-GFP particles and each of these markers

240   using super resolution microscopy (**Fig. 2 *D*** and ***E***). Antibody treatment with $^{ch}\alpha$-GA_3

241   showed a trend (p = 0.08) in favoring the colocalization of GA_{50}-GFP with late endosomes

242   compared to treatment with the IgG isotype control. Indeed 22 % of GA_{50}-GFP vesicles were

243   colocalized with Rab7 in cells treated with $^{ch}\alpha$-GA_3 compared to 12.7 % in cells treated with

244   the IgG isotype control (**Fig. 2*E***). Localization of GA_{50}-GFP in lysosomes was not affected

245   (p = 0.54) (**Fig. 2*E***).

10

246   Taken together, these data demonstrate that α-GA antibodies entered cells and engaged

247   intracellular poly-GA, the presence of which enhanced antibody uptake or intracellular

248   retention. Antibody and GA_{50}-GFP were found in similar intracellular vesicles, with no

249   significant changes of GA_{50}-GFP localization induced by ^{ch}α-GA_3 antibody treatment.

Long-term antibody treatment in human neurons modulates poly-GA solubility by

forming extracellular immune complexes

252   To determine whether chronic antibody treatment can modulate the aggregation state of poly-

253   GA or trigger the aggregate clearance, we added ^{ch}α-GA_1, ^{ch}α-GA_3 or IgG isotype control

254   antibodies to the culture medium of human neural culture transduced with inducible GA_{50}-

255   GFP. After 3, 7 or 21 days of poly-GA induction and simultaneous antibody treatment, cells

256   were either fixed for immunofluorescence imaging followed by aggregate count or lysed for

257   biochemical analysis (**Fig. 3***A*). Without antibody addition, only a faint, diffused or fine

258   punctate GA_{50}-GFP signal was detectable in the cytoplasm 3 days after induction (*SI*

259   *Appendix,* **Fig. S9***A*). By 7 days, GA_{50}-GFP either formed round and bright particles

260   reminiscent of aggregates, or less bright and irregularly shaped structures resembling pre-

261   inclusions (**Fig. 3***B*, *SI Appendix,* **Fig. S9***A*). At 21 days, both aggregates and pre-inclusions

262   increased in number (**Fig 3***C*, *SI Appendix,* **Fig. S9***A*). Quantification confirmed the time-

263   dependent increase of GA_{50}-GFP intracellular inclusions (**Fig 3***C*, gray bars), which remained

264   unaffected by the addition of ^{ch}α-GA_1 (**Fig. 3***C*), or ^{ch}α-GA_3 (*SI Appendix,* **Fig. S9***B*) into the

265   cell culture medium.

266   Interestingly, the addition of ^{ch}α-GA_1 (**Fig. 3***B* and *D*) and ^{ch}α-GA_3 antibodies (*SI Appendix,*

267   **Fig. S9***C*), but not of the IgG isotype control (**Fig. 3***B* and *D*), markedly increased the

268   presence of extracellular bright, large, irregularly shaped GA_{50}-GFP complexes (**Fig. 3***B*)

269   which colocalized with ^{ch}α-GA_1 (**Fig. 4***E*) or ^{ch}α-GA_3 (SI Appendix, **Fig. S8***D*). Extracellular

270   antibody-poly-GA complexes were stable for at least 7 days after doxycycline was removed

11

271   to suppress new GA_{50}-GFP production (**Fig. 3D**). The formation of extracellular immune

272   complexes was consistent with natural release of poly-GA from cells into the medium (34),

273   as cell counting did not reveal poly-GA or antibody-mediated cell death (**Fig. 3F; *SI**

274   *Appendix***, Fig. S9E**).

275   Biochemical analysis showed that the levels of soluble poly-GA were not different across

276   experimental groups (*SI Appendix,* **Fig. S9F**). On the other hand, poly-GA isolated by

277   detergent solubilization followed by centrifugation (40) and quantified with a filter-

278   retardation assay were markedly increased at all time points in neural cultures incubated with

279    $^{ch}\alpha$-GA_1 (**Fig. 3G** and ***H***) or $^{ch}\alpha$-GA_3 (*SI Appendix,* **Fig. S9G** and ***H***) compared with control

280   samples, supporting the presence of poly-GA/antibody immune complexes.

281   To test whether binding of α-GA antibodies to poly-GA aggregates alter their morphology,

282   we first developed a biochemical method for the purification of GA_{50}-GFP aggregates from

283   transiently transfected HEK293T cells. Extracted GA_{50}-GFP aggregates showed remarkable

284   purity and homogeneity, permitting their characterization via scanning electron microscopy

285   (SEM) (**Fig. 3I**). GA_{50}-GFP-expressing HEK293T cellular extracts were incubated with

286   human Alexa Fluor 647-labelled α-GA_1, α-GA_3 or IgG isotype control antibodies, followed

287   by poly-GA aggregate purification, brightfield, immunofluorescence and SEM imaging to

288   eventually carry out correlative light-electron microscopy (CLEM) (**Fig. *S10A-N***). We then

289   assessed and quantified the direct effects of antibody binding on the formation of poly-GA

290   aggregates. Untreated or IgG isotype control-treated poly-GA aggregates appeared

291   consistently spherical and with regular surface pores (**Fig. 3K**). In contrast, binding of either

292   α-GA_1 or α-GA_3 antibodies to poly-GA aggregates altered their morphology and yielded

293   aggregates with a smoother surface (**Fig. 3K-L**). Antibody binding had no effect on the size

294   of the poly-GA spheres, which ranged roughly between 10 and 40 μm^2 (**Fig. 3M**). These

295   results indicate that antibody binding directly alters the biochemical and potentially

296   biological properties of GA_{50}-GFP aggregates, which may affect their toxicity and spreading

297   potential.

298   Overall, antibodies against poly-GA engaged extracellular GA_{50}-GFP into detectable poly-

299   GA/antibody immune complexes, without affecting soluble GA_{50}-GFP levels or poly-GA

300   intracellular structures, while they altered GA_{50}-GFP aggregate formation and morphology in

301   cellular extracts, potentially via stabilization of the poly-GA molecules within the aggregates.

Pharmacokinetics and brain penetration of human-derived antibodies peripherally

administered in $C9^{450}$ mice

304   To test the therapeutic potential of antibodies with high affinity and specificity against poly-

305   GA and poly-GP, three antibodies were selected for investigation in two different G_4C_2-

306   expressing mouse models. The pharmacokinetic and antibody brain penetration properties of

307   human-derived α-GA_1, α-GA_3 or α-GP_1 antibodies were determined after a single

308   intraperitoneal (i.p.) injection of 30 mg/kg of antibodies to transgenic mice expressing a

309   human bacterial artificial chromosome (BAC) with 450 G_4C_2 repeats ($C9^{450}$) (37) (*SI*

310   *Appendix,* **Fig. S11A-D**). The maximum concentrations (C_{max}) in the plasma were 565±30,

311   338±24 and 587±54 µg/ml with estimated terminal elimination half-lives ($t_{1/2}$) of 10.8, 11.0

312   and 7.2 days for α-GA_1, α-GA_3 and α-GP_1, respectively. The corresponding C_{max} in the brain

313   were 0.41±0.16, 0.12±0.07 and 0.28±0.09 µg/mg of total brain protein measured at 2 days

314   post-injection. All antibodies were undetectable by three weeks post-administration. The ratio

315   of the brain drug concentration to the plasma concentration measured at 2 days post-injection

316   was of 0.05-0.1 %, consistent with previous reports for systemically administered antibodies

317   (41). Immunofluorescence using human-specific IgG secondary antibodies did not detect α-

318   GA_1, α-GA_3 and α-GP_1 antibodies 10 days after a single i.p. injection in 20-month-old $C9^{450}$

319   mouse brains having accumulated poly-GA aggregates (*SI Appendix,* **Fig. S11E**).

13

320   **Chronic administration of human-derived antibodies modulates poly-GA solubility**

321   **without significantly altering poly-GA levels in $C9^{450}$ mice**

322   To evaluate the effect of antibodies on the development of DPR pathology in mouse brain,

323   antibodies were intraperitoneally injected in $C9^{450}$ mice from 3 to 19 months of age (**Fig. 4A**).

324   To circumvent the mouse immune response towards the chronic administration of human

325   antibodies we used murine IgG_{2a} chimeric derivatives of the human antibodies. Chimeric α-

326   GA antibodies (^{ch}α-GA$_1$, ^{ch}α-GA$_3$) and α-GP antibody (^{ch}α-GP$_1$) were administered once a

327   week at 30 mg/kg in $C9^{450}$ mice starting at 3 months of age (**Fig. 4A**). The poly-GA

328   aggregate load detectable by immunohistochemistry in $C9^{450}$ mice was too low and variable

329   in this cohort to be reliably quantified. Levels of soluble poly-GA and poly-GP were

330   measured at 7 months of age by immunoassay after sonication of brain homogenates in the

331   presence of 2 % SDS (37) (*SI Appendix,* **Fig. S12A**, fraction 1) from $C9^{450}$ mice expressing

332   comparable levels of the transgene (*SI Appendix,* **Fig. S12B**). Insoluble fractions obtained by

333   ultracentrifugation and resuspension of the corresponding pellet in 7 M Urea (*SI Appendix,*

334   **Fig. S12A,** fraction 2) were measured using similar immunoassays. Soluble poly-GP did not

335   significantly differ between treatment groups (*SI Appendix,* **Fig. S12C**). Poly-GA proteins,

336   however, were not detectable in mice treated with ^{ch}α-GA$_1$ and ^{ch}α-GA$_3$ and were

337   significantly reduced in mice treated with ^{ch}α-GP$_1$ (an antibody recognizing poly-GA with

338   lower affinity; *SI Appendix,* **Fig. S1A** and **S4B**) compared to mice injected with saline only

339   (*SI Appendix,* **Fig. S12D**). This observation suggests that α-GA antibodies interfere with the

340   detection of poly-GA in immunoassays that do not include denaturation of the samples, likely

341   by masking of the epitopes by the injected antibody (**Fig. 4B**, left panel). In addition, while

342   poly-GA was normally not detected in the urea-insoluble fraction from saline injected $C9^{450}$

343   mice (*SI Appendix,* **Fig. S12E,** $C9^{450}$ PBS), poly-GA was present in the insoluble fraction

344   from mice treated with ^{ch}α-GA$_1$ or ^{ch}α-GA$_3$ antibodies (*SI Appendix,* **Fig. S12E,** fraction 2).

345 Notably, similar results were obtained when antibodies were directly spiked into mouse brain

346 homogenates further confirming that poly-GA antibodies form immune complexes with poly-

347 GA that migrate in insoluble fractions and interfere with immunoassay's detection when

348 samples are not efficiently denatured (*SI Appendix,* **Fig. S12*F-H***).

349 To accurately investigate the effect of antibody treatment on poly-GA levels, we adapted the

350 protocol by denaturing any carry-over antibody that might interfere with the poly-GA

351 immunoassay using resuspension in SDS/tris(2-carboxyethyl)phosphine (TCEP) and boiling

352 of the samples (**Fig. 4*B***, right panel, and **Fig. 4*C***). The samples were also subjected to

353 centrifugation and ultracentrifugation after homogenization in 1 % TX100 and 0.25 %

354 deoxycholate (DOC) (**Fig. 4*C***) (1). Denaturation of the brain homogenates demonstrated that

355 poly-GA levels were unchanged between the different treatment groups in the first

356 supernatant fraction (S1) (**Fig. 4*D***). Consistent with our previous results (*SI Appendix,* **Fig.**

357 **S12*E*,** fraction 2), both $^{ch}\alpha$-GA$_1$ and $^{ch}\alpha$-GA$_3$ i.p. injections in C9^{450} mice increased the

358 presence of poly-GA in the pellet fraction (P2) after ultracentrifugation (**Fig. 4E**), supporting

359 the presence of poly-GA/antibody immune complexes.

360 **Chronic administration of human-derived antibodies modulates poly-GA solubility and**

361 **increases poly-GA levels in AAV(G$_4$C$_2$)$_{149}$ mice**

362 The impact of $^{ch}\alpha$-GA$_1$ antibody was also determined in somatic transgenic mice generated

363 by intra-cerebroventricular (ICV) administration to post-natal day 0 mice of adeno-associated

364 virus encoding either 2 or 149 G$_4$C$_2$ hexanucleotide repeats [AAV(G$_4$C$_2$)$_2$ or AAV(G$_4$C$_2$)$_{149}$]

365 (**Fig. 4*F***). Weekly i.p. injections of $^{ch}\alpha$-GA$_1$ or the IgG isotype control were carried out from

366 2 to 12 months of age and brains were collected either at 4 or at 12 months of age for poly-

367 GA and poly-GP measurements (**Fig. 4*G-L***). Using an immunoassay that included

368 denaturation of the samples, we identified a significantly increased accumulation of poly-GA

15

369 in the supernatant S1 fraction in AAV$(G_4C_2)_{149}$ mice treated with $^{ch}\alpha$-GA$_1$ compared to mice

370 injected with the IgG control at 4 (**Fig. 4G**) and 12 months *(Fig. 4I).* After ultracentrifugation

371 of the samples, the levels of poly-GA in protein fractions S2 and P2 were not changed at 4

372 months of age (**Fig. 4H**), but were significantly increased in all fractions from 12-month-old

373 mice treated with $^{ch}\alpha$-GA$_1$ compared to mice injected with the IgG control (**Fig. 4J**). On the

374 contrary, poly-GP solubility and levels were unaltered by $^{ch}\alpha$-GA$_1$ treatment (**Fig. 4K** and *L*).

375 In addition, sarkosyl-insoluble pellets isolated via SarkoSpin (40) from total brain

376 homogenates of 4-month-old AAV(G_4C_2) mice were analyzed via filter retardation assay (*SI*

377 *Appendix,* **Fig. S13A** and *B*). $^{ch}\alpha$-GA$_1$ antibody was specifically retained on the membrane in

378 the $^{ch}\alpha$-GA$_1$-treated AAV$(G_4C_2)_{149}$ mouse samples suggesting that the non-denaturing

379 conditions of the SarkoSpin protocol led to the isolation of sarkosyl-insoluble $^{ch}\alpha$-GA$_1$

380 antibody-poly-GA complexes, which were not observed with IgG isotype control (*SI*

381 *Appendix,* **Fig. S13A** and *B*). Insoluble, poly-ubiquitinated proteins were detected in both

382 AAV$(G_4C_2)_{149}$ mouse conditions and their levels were not affected by $^{ch}\alpha$-GA$_1$ antibody

383 treatment (*SI Appendix,* **Fig. S13C** and *D*).

384 **Chronic administration of human-derived antibodies did not impact poly-GA aggregate**

385 **load in AAV$(G_4C_2)_{149}$ mice**

386 By 4 months of age, AAV$(G_4C_2)_{149}$ mice accumulated large perinuclear poly-GA aggregates

387 throughout the brain that co-localized with poly-GR and poly-GP (*SI Appendix,* **Fig. S14A**

388 and *B*), as observed in postmortem tissues from patients (7). We determined the area

389 occupied by poly-GA aggregates in AAV$(G_4C_2)_{149}$ mice treated for 2 or 10 months with $^{ch}\alpha$-

390 GA$_1$ antibody compared to mice treated with the IgG isotype control. To test whether

391 treatment with α-GA antibodies may interfere with detection of aggregates (as observed in

392 immunoassays without strong denaturation; **Fig. 4B**, *SI Appendix,* **Fig. S12D** and *G*),

393 immunofluorescence was performed using either an antibody raised against poly-GA (37) or

16

394   an antibody raised against a N-terminal peptide starting at a CUG initiation codon in the

395   poly-GA frame (10). When using an anti-GA antibody to detect aggregates there was no

396   change in the poly-GA aggregates after 2 months of treatment (*SI Appendix,* **Fig. S14C** and

397   ***D***), but the area appeared significantly decreased in the cortex after 10 months of treatment

398   with $^{ch}\alpha$-GA$_1$ antibody (*SI Appendix,* **Fig. S14E**). A non-significant similar trend was

399   observed in the hippocampus (*SI Appendix,* **Fig. S14F**). However, this reduction was not

400   observed when we used an antibody raised against the N-terminal peptide of poly-GA (**Fig.**

401   **5A-C**), demonstrating the importance of using antibodies that recognize different epitopes

402   than the treatment antibody when assessing the effect of an immunotherapy against poly-GA.

403   As expected, poly-GP aggregates were not affected in either the cortex (**Fig. 5D** left panels,

404   and **Fig. 5E**) or the hippocampus (**Fig. 5D** right panels, and **Fig. 5F**). The level of poly-GR

405   measured by immunoassay (*SI Appendix,* **Fig. S14G**) and the area of poly-GR aggregates (*SI*

406   *Appendix,* **Fig. S14H**) were also not modified by treatment with $^{ch}\alpha$-GA$_1$ antibody. Similarly,

407   the number of phospho-TDP-43 aggregates detected by immunohistochemistry in

408   AAV(G$_4$C$_2$)$_{149}$ mice was not altered by treatment with $^{ch}\alpha$-GA$_1$ (*SI Appendix,* **Fig. S15A** and

409   ***B***).

410   **Long-term *in vivo* administration of DPR antibodies was well tolerated with a modest**

411   **impact on behavior in C9^{450} mice**

412   C9^{450} mice were treated by weekly injection of $^{ch}\alpha$-GA$_1$, $^{ch}\alpha$-GA$_3$ and $^{ch}\alpha$-GP$_1$ from 3 to 19

413   months of age (**Fig. 4A**). Antibody titers in serum (measured every 2 months, 24 hrs after

414   injection) remained stable over time (*SI Appendix,* **Fig. S16A-C**). Chronic administration did

415   not result in any obvious adverse effects, with comparable survival (**Fig. 6A**) and body

416   weight (*SI Appendix,* **Fig. S16D** and ***E***) between the different treatment groups,

417   demonstrating the tolerability of all three antibodies at 30 mg/kg per week for 16 months. At

17

418 13 months of age, only $C9^{450}$ males exhibited a decreased activity with a significant reduction

419 in distance moved compared to age-matched wild-type mice in an open-field assay (*SI*

420 *Appendix,* **Fig. S16F**). At this age, these differences were not impacted by $^{ch}\alpha$-GA_1, $^{ch}\alpha$-GA_3

421 and $^{ch}\alpha$-GP_1 antibody treatment (*SI Appendix,* **Fig. S16F**). However, by 18 months of age,

422 $C9^{450}$ mice treated with PBS continued to display a significantly decreased activity compared

423 to wild-type animals, while mice treated with $^{ch}\alpha$-GA_3 showed a significant rescue when

424 compared to $C9^{450}$ animals treated with PBS (p=0.0149) (**Fig. 6B**). Mice treated with $^{ch}\alpha$-GA_1

425 and $^{ch}\alpha$-GP_1 antibodies also showed a non-significant trend towards improvement in this

426 behavioral assay (**Fig. 6B**). As previously reported (37), $C9^{450}$ mice develop a loss of

427 hippocampal neurons that was not significantly alleviated by treatment with DPR antibodies

428 (**Fig. 6C**).

429 **Long-term *in vivo* administration of DPR antibodies did not significantly impact disease**

430 **progression in AAV$(G_4C_2)_{149}$ mice**

431 AAV$(G_4C_2)_{149}$ mice were treated by weekly i.p. injection of $^{ch}\alpha$-GA_1 at 30 mg/kg from 2 to

432 12 months of age (**Fig. 4E**). The survival of these mice was not impacted by the expression of

433 the G_4C_2 repeats as previously described (42) and antibody treatment was well tolerated (**Fig.**

434 **6D** and *SI Appendix,* **Fig. S16G-H**). AAV$(G_4C_2)_{149}$ mice presented abnormal activity

435 including increases in distance traveled and velocity of movement, and time spent moving on

436 an open-field assay compared to control AAV$(G_4C_2)_2$ mice (**Fig. 6E-G**). These phenotypes

437 were not impacted by chronic administration of $^{ch}\alpha$-GA_1 antibody. When assessing strength

438 by measuring the ability to cling on an inverted metal grid, female AAV$(G_4C_2)_{149}$ mice

439 showed significantly lower performance compared to AAV$(G_4C_2)_2$ mice (p = 0.002) (**Fig.**

440 **6H**). Although there was a trend towards improvement, the deficit in AAV$(G_4C_2)_{149}$ mice

441 was not significantly rescued by $^{ch}\alpha$-GA_1 treatment (p = 0.11). In addition, treatment with $^{ch}\alpha$-

18

442   GA_1 did not impact the decrease in brain weight observed in $AAV(G_4C_2)_{149}$ mice compared

443   to $AAV(G_4C_2)_2$ mice (**Fig. 6I**).

444

445   **Discussion**

446   In this study, we have characterized potential immunotherapies (based on human antibodies)

447   for C9ORF72-related ALS and FTD. Eleven antibodies against all five C9ORF72 DPR

448   species were identified and systematically characterized. The exact trigger(s) leading to the

449   production of antibodies against DPRs in healthy people is unknown. It is conceivable that

450   due to their highly repetitive sequences, DPRs may present sequence or structural similarities

451   with other antigens potentially derived from bacteria or viruses. Alternatively, the 2 to 30

452   (G_4C_2) repeats found in the normal population may produce DPR proteins at a very low rate,

453   which may trigger an antibody-mediated immune response without being pathogenic. While

454   we have systematically characterized antibodies against each C9ORF72-related DPR, we

455   focused on antibodies against poly-GA, recognizing that this DPR is the most abundant with

456   high aggregation propensity in ALS/FTD human autopsy brain samples (7, 43) and with

457   strong neurotoxicity in mice (20, 23). Moreover, poly-GA has the ability to trap other DPR

458   species and modulate C9ORF72 toxicity observed in multiple cellular and animal models (21,

459   22, 24).

460   While antibody treatment against intracellular Tau and α-synuclein are currently being tested

461   for Alzheimer's and Parkinson's diseases respectively (28, 29, 33), the exact mechanisms of

462   action of immunotherapy against intracellular proteins remain unclear. Antibodies were

463   shown to either facilitate clearance of the target or to prevent spreading and toxicity. The

464   tested α-GA antibodies were robustly internalized by poly-GA-expressing human neurons, a

465   finding in line with published studies showing antibody uptake by neuronal cells (35, 36). In

466   this cellular model, intracellular antibodies colocalized with poly-GA in cytoplasmic puncta,

467   however, less prominently to very dense and large intracellular aggregates formed over time.

468   It is possible that their compact structure may conceal the epitope recognized by the antibody.

469   Alternatively, poly-GA physical associations with other proteins may interfere with epitope

470   recognition. Antibody and poly-GA colocalized partially with late-endosomes and lysosomes,

471   but anti-GA antibody treatment did not significantly alter GA_{50}-GFP vesicular localization.

472   Whether antibody and antigen entered the same degradation pathway independently, or

473   antibody binding on poly-GA triggered its engulfment in endocytic vesicles, thereby

474   potentially stimulating its clearance remains unanswered. It is also possible that the antibodies

475   engaged the poly-GA extracellularly and entered human neurons already as a complex.

476   However, the absence of antibody-engaged poly-GA in non-transduced, wild-type neurons

477   present in the same neuronal network challenges that notion. Rather, as supported by super

478   resolution microscopy, the dense GA_{50}-GFP inclusions and aggregates may be present in a

479   different compartment than the antibody-engaged poly-GA. Notably, despite target

480   engagement in our cellular models and reduction of poly-GA aggregates in T98G anchorage

481   independent cancer cell line, intracellular GA_{50}-GFP inclusions and aggregates were not

482   affected by antibody treatment in cultured human neurons, highlighting differences between

483   cell types.

484   Of note, the three cellular models used in this study were differently modified to overexpress

485   poly-GA. While the liposome-mediated transfection of SH-SY5Y cells may have indirectly

486   enhanced the antibody "uptake" because of partially compromised cell membrane, both the

487   T98G cells (stable transfection) and human neurons (lentivirus-mediated gene delivery and

488   cell recovery for several days before antibody treatment) likely had intact cell membrane and

489   thus accurately modeled antibody uptake and/or retention in cancer cells or human neurons,

490   respectively. Interestingly, anti-GA antibodies did engage less prominently the dense poly-

491   GA aggregates in human neurons synthetizing poly-GA, compared to their targeting of

492   aggregates in stably transfected T98G cancer cells. This points to a distinct aggregate

493   handling between cycling cells and differentiated neurons. In addition, IF experiments with

494   fixed and permeabilized motor neuron-like NSC-34 cells overexpressing poly-GA via

495   transient transfection revealed that all tested anti-GA antibodies (α-GA$_{1-4}$) only partially

496   recognized dense poly-GA aggregates.

497   It was previously shown that poly-GA is released into the extracellular space and can be

498   taken up by neighboring cells, thereby increasing DPR aggregation (22, 32, 34). A similar

499   mechanism may account for spreading of DPR pathology throughout the nervous system, as

500   was hypothesized for other intracellular protein aggregates found in ALS/FTD (44), a process

501   that may be blocked by immunotherapy. We showed that human-derived antibodies

502   efficiently captured extracellular poly-GA over the course of 3 weeks forming large immune

503   complexes in human neuronal cultures. This was also described in the context of Alzheimer's

504   disease, where an anti-Tau antibody blocked toxicity and spreading through the formation of

505   immune complexes (45). We were unable to assess whether the formation of poly-

506   GA/antibody immune complexes could rescue poly-GA toxicity in this cellular system, since

507   we found no detectable poly-GA toxicity within the time course of 21 days.

508   In contrast to previous studies that reported a decrease in intracellular aggregates and

509   insolubility of poly-GA upon α-GA treatment in cells (1, 32), our analysis in cultured human

510   neurons did not find a decrease of intracellular inclusions and showed a significant increase

511   of poly-GA insolubility, likely due to the formation of immune complexes (**Fig. 3**).

512   Antibody-induced insolubility has been previously reported for α-synuclein, which formed

513   amorphous aggregates *in vitro* in the presence of four out of six tested α-synuclein antibodies

514   (46). In comparison to α-synuclein, which has a strong ability to form fibrils (46), the

515   unusually high hydrophobic and low complexity nature of poly-GA (7, 15) may make it more

516   prone to clump into amorphous aggregates when molecules are brought into close proximity

21

517   following antibody binding. An antibody selective for soluble Tau triggered the formation of

518   extracellular complexes and protected against exogenous paired helical filament toxicity,

519   while an alternative antibody directed against aggregated Tau failed at forming extracellular

520   immune complexes and could not confer cellular protection (45).

521   We also observed that the detection of poly-GA either by immunoassay or by

522   immunofluorescence staining was altered by treatment with anti-GA antibodies. Indeed,

523   using an antibody that does not recognize the poly-GA epitopes but rather a N-terminal

524   peptide translated in frame with poly-GA (10), we demonstrated that poly-GA aggregates

525   were not affected by 9 months of $^{ch}\alpha$-GA$_1$ treatment in AAV(G$_4$C$_2$)$_{149}$ mice (**Fig. 5**).

526   However, the aggregate load appeared reduced when immunostaining was performed using

527   an antibody against poly-GA (*SI Appendix,* **Fig. S14E**), suggesting that the treatment with

528     $^{ch}\alpha$-GA$_1$ antibody may block the recognition of poly-GA epitopes by the detecting antibody

529   leading to underestimation of poly-GA aggregates. The vast majority, if not all, of poly-GA

530   is translated from a start codon located 24 nucleotides upstream of the repeat that encode the

531   N-terminal peptide (10, 47). Hence, it is unlikely that the poly-GA species detected by the N-

532   terminal peptide directed-antibody represent only a subset of poly-GA that would be

533   differently impacted by the treatment. In addition, an interference between the treatment and

534   detection antibodies was demonstrated in a biochemical assay lacking efficient denaturation

535   of the samples before poly-GA measurement (*SI Appendix,* **Fig. S12**). Such an interference

536   was not observed for the uncharged, flexible and highly soluble (48) poly-GP molecules (*SI*

537   *Appendix,* **Fig. S12C**) suggesting that intrinsic structural features of poly-GA are altered by

538   antibody recognition, as supported by our SEM analysis of purified poly-GA (**Fig. 3I-M**).

539   Combined with the robust formation of poly-GA-antibody complexes evident in all our

540   cellular work, these changes highlight the necessity of analyzing all biochemical fractions

541   when comparing antibody-treated to non-treated conditions. While interference between the

542 treatment and detecting antibodies or antibody-induced biochemical changes may not be an

543 issue for all proteins, our study demonstrates that careful denaturation of biochemical

544 samples and use of antibodies recognizing independent epitopes is warranted for accurate

545 assessment of the impact of immunotherapies on aggregation-prone proteins.

546 In this study, we have not observed a reversal of the clinical phenotypes linked to C9ORF72

547 disease in our antibody-treated $AAV(G_4C_2)_{149}$ mice. This is contrary to a recently published

548 study in a C9ORF72 BAC model (1). The reason for this discrepancy in response to the

549 antibody treatment is unknown – one possibility is that the different mouse models used in

550 the two studies display different phenotypes resulting in differential responses to antibody

551 treatment. Alternatively, the discrepancy may be linked to the fact that in contrast to other

552 described mouse models expressing G_4C_2 C9ORF72 repeats (37, 38, 42, 49, 50), the model

553 used in the Nguyen et al. study has been reported to develop severe neurodegeneration (1).

554 Mordes et al (51) described that two independent cohorts of the same model had similar

555 levels of DPRs but did not have the same behavioral phenotypes previously reported in these

556 mice. While independent laboratories reproduced the originally reported phenotypes in the

557 C9ORF72 BAC mouse model (52), Mordes and colleagues (51) proposed that the severe

558 neurodegeneration reported in a fraction of the mice used by Nguyen and colleagues may be

559 linked to the space cadet syndrome (SCS), previously reported in WT mice with an FVB/N

560 background (53). While C9ORF72-linked neurodegeneration may be exacerbated by – and

561 potentially distinguished from – the severe seizure phenotypes affecting both C9ORF72 and

562 non-transgenic animals (52), future studies are necessary to determine the relative

563 contribution(s) of the *C9ORF72* repeat expansion, the DPR expression levels and the SCS-

564 linked pathologies to the described phenotypes and their immunotherapy-driven reversal in

565 different mouse models.

23

566   In the current study, we have not observed target engagement by IHC in the brains of our

567     $C9^{450}$ antibody-treated mice. We have observed constant antibody plasma titers over 1.5

568   years with brain penetration of a small fraction (~0.1 %) of the injected antibody (as

569   previously shown (25) for other antibodies), but peripherally injected human antibodies were

570   not found to co-localize with neuronal poly-GA aggregates (*SI Appendix,* **Fig. S11***E*). The

571   reason for this difference from the observations in Nguyen et al. (1) is unclear, but it is

572   conceivable that the severe neurodegeneration and/or SCS pathology in the mice used by

573   Nguyen et al. may be associated with blood-brain barrier leakage, which might facilitate

574   antibody entry to the brain. Whether that accounts for the reported decrease in poly-GA load

575   in these mice remains to be clarified.

576   In our $C9^{450}$ cohort, the levels of poly-GA and poly-GP could be measured by immunoassay

577   but the number of poly-GA aggregates were too low to evaluate the effect of antibody

578   treatment on poly-GA aggregate load. Despite the lack of widespread poly-GA pathology,

579   long term treatment with anti-GA antibodies improved an open field movement test in aged

580     $C9^{450}$ mice (albeit modestly). In $AAV(G_4C_2)_{149}$ mice, anti-GA treatment failed to ameliorate

581   brain atrophy and poly-GA levels increased following treatment during 9 months. This

582   finding supports that at least a small portion of peripherally injected antibodies accessed

583   poly-GA in the brain and impacted its turn-over. Targeting some of the other reportedly toxic

584   DPR proteins, such as poly-GR and poly-PR, may be an alternative and potentially

585   synergistic approach to treat *C9orf72* disease which should be explored in future studies.

586   Furthermore, we anticipate that antibody delivery is key for the success of immunotherapy

587   and approaches to increase antibody penetration to the central nervous system (54) might

588   result in enhanced therapeutic benefit.

589

References:

1. Nguyen L, *et al.* (2020) Antibody Therapy Targeting RAN Proteins Rescues C9 ALS/FTD Phenotypes in C9orf72 Mouse Model. *Neuron* 105(4):645-662 e611.

2. Zhou Q, *et al.* (2020) Active poly-GA vaccination prevents microglia activation and motor deficits in a C9orf72 mouse model. *EMBO Mol Med* 12(2):e10919.

3. Renton A, *et al.* (2011) A hexanucleotide repeat expansion in C9ORF72 is the cause of chromosome 9p21-linked ALS-FTD. *Neuron* 72:257 - 268.

4. DeJesus-Hernandez M, *et al.* (2011) Expanded GGGGCC hexanucleotide repeat in noncoding region of C9ORF72 causes chromosome 9p-linked FTD and ALS. *Neuron* 72:245 - 256.

5. Taylor JP, Brown RH, Jr., & Cleveland DW (2016) Decoding ALS: from genes to mechanism. *Nature* 539(7628):197-206.

6. Ash PE, *et al.* (2013) Unconventional translation of C9ORF72 GGGGCC expansion generates insoluble polypeptides specific to c9FTD/ALS. *Neuron* 77(4):639-646.

7. Mori K, *et al.* (2013) The C9orf72 GGGGCC Repeat Is Translated into Aggregating Dipeptide-Repeat Proteins in FTLD/ALS. *Science* 339(6125):1335-1338.

8. Zu T, *et al.* (2011) Non-ATG-initiated translation directed by microsatellite expansions. *Proc Natl Acad Sci U S A* 108(1):260-265.

9. Gendron TF, *et al.* (2013) Antisense transcripts of the expanded C9ORF72 hexanucleotide repeat form nuclear RNA foci and undergo repeat-associated non-ATG translation in c9FTD/ALS. *Acta Neuropathol* 126(6):829-844.

10. Tabet R, *et al.* (2018) CUG initiation and frameshifting enable production of dipeptide repeat proteins from ALS/FTD C9ORF72 transcripts. *Nat Commun* 9(1):152.

11. Cheng W, *et al.* (2018) C9ORF72 GGGGCC repeat-associated non-AUG translation is upregulated by stress through eIF2alpha phosphorylation. *Nat Commun* 9(1):51.

12. Gendron TF, *et al.* (2015) Cerebellar c9RAN proteins associate with clinical and neuropathological characteristics of C9ORF72 repeat expansion carriers. *Acta Neuropathologica* 130(4):559-573.

13. Mann DM, *et al.* (2013) Dipeptide repeat proteins are present in the p62 positive inclusions in patients with frontotemporal lobar degeneration and motor neurone disease associated with expansions in C9ORF72. *Acta Neuropathologica Communications* 1(1):68.

14. Al-Sarraj S, *et al.* (2011) p62 positive, TDP-43 negative, neuronal cytoplasmic and intranuclear inclusions in the cerebellum and hippocampus define the pathology of C9orf72-linked FTLD and MND/ALS. *Acta Neuropathol* 122(6):691-702.

15. Kwon I, *et al.* (2014) Poly-dipeptides encoded by the C9ORF72 repeats bind nucleoli, impede RNA biogenesis, and kill cells. *Science*.

16. Mizielinska S, *et al.* (2014) C9orf72 repeat expansions cause neurodegeneration in Drosophila through arginine-rich proteins. *Science*.

17. Lee KH, *et al.* (2016) C9orf72 Dipeptide Repeats Impair the Assembly, Dynamics, and Function of Membrane-Less Organelles. *Cell* 167(3):774-788 e717.

18. Shi KY, *et al.* (2017) Toxic PRn poly-dipeptides encoded by the C9orf72 repeat expansion block nuclear import and export. *Proc Natl Acad Sci U S A* 114(7):E1111-E1117.

19. Lin Y, *et al.* (2016) Toxic PR Poly-Dipeptides Encoded by the C9orf72 Repeat Expansion Target LC Domain Polymers. *Cell* 167(3):789-802 e712.

20. Zhang YJ, *et al.* (2016) C9ORF72 poly(GA) aggregates sequester and impair HR23 and nucleocytoplasmic transport proteins. *Nat Neurosci* 19(5):668-677.

21. Guo Q, *et al.* (2018) In Situ Structure of Neuronal C9orf72 Poly-GA Aggregates Reveals Proteasome Recruitment. *Cell* 172(4):696-705 e612.

22. Chang YJ, Jeng US, Chiang YL, Hwang IS, & Chen YR (2016) The Glycine-Alanine Dipeptide Repeat from C9orf72 Hexanucleotide Expansions Forms Toxic Amyloids Possessing Cell-to-Cell Transmission Properties. *J Biol Chem* 291(10):4903-4911.

23. LaClair KD, *et al.* (2020) Congenic expression of poly-GA but not poly-PR in mice triggers selective neuron loss and interferon responses found in C9orf72 ALS. *Acta Neuropathol* 140(2):121-142.

24. Brody DL & Holtzman DM (2008) Active and Passive Immunotherapy for Neurodegenerative Disorders. *Annual Review of Neuroscience* 31(1):175-193.

25. Sevigny J, *et al.* (2016) The antibody aducanumab reduces Abeta plaques in Alzheimer's disease. *Nature* 537(7618):50-56.

26. Rinne JO, *et al.* (2010) 11C-PiB PET assessment of change in fibrillar amyloid-beta load in patients with Alzheimer's disease treated with bapineuzumab: a phase 2, double-blind, placebo-controlled, ascending-dose study. *Lancet Neurol* 9(4):363-372.

27. Kastanenka KV, *et al.* (2016) Immunotherapy with Aducanumab Restores Calcium Homeostasis in Tg2576 Mice. *J Neurosci* 36(50):12549-12558.

28. Boutajangout A, Quartermain D, & Sigurdsson EM (2010) Immunotherapy targeting pathological tau prevents cognitive decline in a new tangle mouse model. *J Neurosci* 30(49):16559-16566.

29. Yanamandra K, *et al.* (2013) Anti-tau antibodies that block tau aggregate seeding in vitro markedly decrease pathology and improve cognition in vivo. *Neuron* 80(2):402-414.

30. Masliah E, *et al.* (2005) Effects of alpha-synuclein immunization in a mouse model of Parkinson's disease. *Neuron* 46(6):857-868.

31. Maier M, *et al.* (2018) A human-derived antibody targets misfolded SOD1 and ameliorates motor symptoms in mouse models of amyotrophic lateral sclerosis. *Sci Transl Med* 10(470).

32. Zhou Q, *et al.* (2017) Antibodies inhibit transmission and aggregation of C9orf72 poly-GA dipeptide repeat proteins. *EMBO Mol Med* 9(5):687-702.

33. Tran HT, *et al.* (2014) Alpha-synuclein immunotherapy blocks uptake and templated propagation of misfolded alpha-synuclein and neurodegeneration. *Cell Rep* 7(6):2054-2065.

34. Westergard T, *et al.* (2016) Cell-to-Cell Transmission of Dipeptide Repeat Proteins Linked to C9orf72-ALS/FTD. *Cell Rep* 17(3):645-652.

35. Congdon EE, Gu J, Sait HB, & Sigurdsson EM (2013) Antibody uptake into neurons occurs primarily via clathrin-dependent Fcgamma receptor endocytosis and is a prerequisite for acute tau protein clearance. *J Biol Chem* 288(49):35452-35465.

36. Gustafsson G, *et al.* (2017) Cellular Uptake of alpha-Synuclein Oligomer-Selective Antibodies is Enhanced by the Extracellular Presence of alpha-Synuclein and Mediated via Fcgamma Receptors. *Cell Mol Neurobiol* 37(1):121-131.

37. Jiang J, *et al.* (2016) Gain of Toxicity from ALS/FTD-Linked Repeat Expansions in C9ORF72 Is Alleviated by Antisense Oligonucleotides Targeting GGGGCC-Containing RNAs. *Neuron* 90(3):535-550.

38. Chew J, *et al.* (2015) Neurodegeneration. C9ORF72 repeat expansions in mice cause TDP-43 pathology, neuronal loss, and behavioral deficits. *Science* 348(6239):1151-1154.

39. Hruska-Plochan M, *et al.* (2021) Human neural networks with sparse TDP-43 pathology reveal NPTX2 misregulation in ALS/FTLD. *bioRxiv*:2021.2012.2008.471089.

40. Laferriere F*, et al.* (2019) TDP-43 extracted from frontotemporal lobar degeneration subject brains displays distinct aggregate assemblies and neurotoxic effects reflecting disease progression rates. *Nat Neurosci* 22(1):65-77.

41. Levites Y*, et al.* (2006) Insights into the mechanisms of action of anti-Abeta antibodies in Alzheimer's disease mouse models. *FASEB J* 20(14):2576-2578.

42. Chew J*, et al.* (2019) Aberrant deposition of stress granule-resident proteins linked to C9orf72-associated TDP-43 proteinopathy. *Mol Neurodegener* 14(1):9.

43. Mackenzie IR*, et al.* (2015) Quantitative analysis and clinico-pathological correlations of different dipeptide repeat protein pathologies in C9ORF72 mutation carriers. *Acta Neuropathol* 130(6):845-861.

44. Polymenidou M & Cleveland DW (2011) The seeds of neurodegeneration: prion-like spreading in ALS. *Cell* 147(3):498-508.

45. Congdon EE*, et al.* (2016) Affinity of Tau antibodies for solubilized pathological Tau species but not their immunogen or insoluble Tau aggregates predicts in vivo and ex vivo efficacy. *Mol Neurodegener* 11(1):62.

46. Sahin C*, et al.* (2017) Antibodies against the C-terminus of alpha-synuclein modulate its fibrillation. *Biophys Chem* 220:34-41.

47. Almeida S*, et al.* (2019) Production of poly(GA) in C9ORF72 patient motor neurons derived from induced pluripotent stem cells. *Acta Neuropathol* 138(6):1099-1101.

48. Freibaum BD & Taylor JP (2017) The Role of Dipeptide Repeats in C9ORF72-Related ALS-FTD. *Frontiers in Molecular Neuroscience* 10(35).

49. O'Rourke JG*, et al.* (2015) C9orf72 BAC Transgenic Mice Display Typical Pathologic Features of ALS/FTD. *Neuron* 88(5):892-901.

50. Peters OM*, et al.* (2015) Human C9ORF72 Hexanucleotide Expansion Reproduces RNA Foci and Dipeptide Repeat Proteins but Not Neurodegeneration in BAC Transgenic Mice. *Neuron* 88(5):902-909.

51. Mordes DA*, et al.* (2020) Absence of Survival and Motor Deficits in 500 Repeat C9ORF72 BAC Mice. *Neuron*.

52. Nguyen L*, et al.* (2020) Survival and Motor Phenotypes in FVB C9-500 ALS/FTD BAC Transgenic Mice Reproduced by Multiple Labs. *Neuron*.

53. Ward JM (2000) *Pathology of genetically engineered mice* (Iowa State University Press, Ames) 1st Ed pp xi, 394 p.

54. Bravo-Hernandez M*, et al.* (2020) Spinal subpial delivery of AAV9 enables widespread gene silencing and blocks motoneuron degeneration in ALS. *Nat Med* 26(1):118-130.

732 Analysis with assistance from Johannes Riemann and Andres Kaech (University of Zurich)

733 as well as with microscopes from Rudy Tanzi's and Brian Wainger's laboratories (MGH).

734 Human postmortem tissues were obtained from Matthew Frosch and Jose McLean at the

735 Massachusetts Alzheimer's Disease Research Center (PG50 AG005134).

736 **Funding:** This work was supported by grants from the ALS Association and NINDS/NIH

737 (R01NS087227) to CLT and from Target ALS to CLT and MP. MJ received a doctoral

738 fellowship from the University of Zurich (K-74423-04-01) and a NCCR mobility grant from

739 the Swiss National Science Foundation (51NF40-141735). RT was supported by the Philippe

740 Foundation and FF by an ECOR Tosteson Postdoctoral Fellowship. MHP was supported by a

741 Milton Safenowitz Postdoctoral Fellowship (16-PDF-247), a postdoctoral fellowship from

742 the University of Zurich (FK-15-097) and the Promotor-Stiftung from the Georges and

743 Antoine Claraz Foundation.

744 **Author contribution:** RT, CZL, KDM, MJ, MHP, ARS, NM, CA, PB, KS, NM, NC, PB,

745 SD, ID, CCL, JJ, XJ, JP, SN, YG, SD, IDL, ZM, JW, MW, MM, KS, TG, MP, FM and CLT

746 conducted experiments or analyzed data; KJW, JJ, FF, NL, PDR, MPB, LMD, EB, YZ, JB,

747 BW, MWK, MR, CH, RMN, DWC, LP supplied material and/or gave significant input; MJ,

748 KDM, RT, MHP, ARS, MWK, MR, MP, CLT, FM, JG, DWC, LP wrote or edited the

749 manuscript.

750 **Competing interests:** KDM, NC, PB, CH, RMN, FM, JG are employees of Neurimmune

751 and SN, YG, SD, ID, MWK, MR are employees of Biogen.

752 **Data and materials availabilities:** The data that support the findings of this study are

753 available from the corresponding authors upon request. Constructs and reagents generated in

754 this study can be shared upon request with establishment of an appropriate material transfer

755 agreement. There may be restrictions to the availability of some data/reagents due to

756 agreements with industry partners.

28

757

List of Supplementary Materials:

Materials and Methods

Tables S1, Figure S1-S16

761

762 **Legends**

763

764 **Fig. 1. Antibody uptake and poly-GA colocalization in living cells**

765 **(A)** Confocal fluorescence images of SH-SY5Y cells transfected with GA_{50}-GFP (green) and

766 incubated with human α-GA_1, α-GA_3 or an IgG control antibody (72 hrs). Antibodies were

767 visualized after fixation with a secondary α-human IgG antibody (red) and nuclei with DAPI

768 (blue). Scale = 100 μm. **(B)** Percentage of GA_{50}-GFP area that colocalized with antibody. N =

769 4 biological replicates from 2 independent experiments. Mean value of each replicate

770 calculated from 3 distinct fields. **(C)** Flow cytometry-based approach to quantify the uptake

771 of labeled antibodies into cells transfected with HA-GA_{50} or no plasmid (mock transfected).

772 Membrane-associated antibodies were degraded by trypsin and any remaining extracellular

773 signal was quenched by Trypan Blue. **(D)** HA-GA_{50} or mock transfected SH-SY5Y cells

774 incubated with Alexa 488-labeled α-GA_1, α-GA_3 or the IgG control and analyzed by flow

775 cytometry. Viable, singlet cells were selected for fluorescence negative (grey) or positive

776 (orange, red or black) populations. **(E)** Percentage of antibody-positive cells after 48 hrs.

777 Each data point represents 30,000 cells. N = 3 biological replicates. **(B, E)** Mean ± SD, one-

778 way ANOVA followed by Tukey's multiple comparison test. **(F)** Immunofluorescence of

779 T98G cells expressing GA_{161}-GA (green) and treated with antibody (red) for 72 hrs. **(G, H)**

780 Compared with IgG control-treated cells, α-GA_1-treated cells exhibited a significant

781 reduction in the number of poly-GA aggregates per cell **(G)** and in volume of aggregates per

782 cell **(H)**. N = 3 biological triplicates with 10 or 11 fields captured per replicate. Mean ± SD,

783 unpaired two-tailed t-test. * P ≤ 0.05, ** P ≤ 0.01, *** P ≤ 0.001.

784 **Fig. 2. ^{ch}α-GA$_3$ is internalized *via* vesicular compartments in human neurons, but does**

785 **not alter GA$_{50}$-GFP vesicular localization**

786 **(A)** Confocal images of human neural cultures expressing an inducible GA$_{50}$-GFP construct

787 treated for 3 days with ^{ch}α-GA$_3$ or IgG control, and stained with a secondary α-human

788 antibody (red). White arrows show antibody/GA$_{50}$-GFP double positive cells and arrowheads

789 show antibody uptake in cells not expressing GA$_{50}$-GFP. Scale = 20 μm. **(B)** Quantification

790 of the percentage of GA$_{50}$-GFP expressing cells with internalized antibody. Four replicates,

791 unpaired t-test. *** P < 0.0001. **(C)** Confocal images after staining with either α-RAB7 (late

792 endosomes) or α-LAMP1 (lysosomes) and with α-mouse antibody (red) to detect the

793 chimeric antibodies. **(D**) Deconvoluted STED image from a neuron expressing GA$_{50}$-GFP

794 treated with ^{ch}α-GA$_3$ and stained with RAB7. Inset of the STED image (upper panel) and the

795 created 2D surface (lower panels) are enlarged from the original site (white box). **(E)**

796 Distances between each GA$_{50}$-GFP particle and the closest RAB7 or LAMP1 vesicular

797 markers were measured. The percentage of GA$_{50}$-GFP particles containing a vesicle within a

798 100 nm radius were considered as colocalized with the indicated vesicle. Each dot represents

799 a field of view. Mann and Whitney U test (Rab7 p = 0.087 and Lamp1 p = 0.544).

800 **Fig. 3. Poly-GA and antibodies form large hetero-complexes in long-term treated**

801 **neuronal cultures**

802 **(A)** Experimental strategies to test the effect of antibody treatment on human neurons

803 expressing GA$_{50}$-GFP. **(B)** Immunofluorescence showing GA$_{50}$-GFP in neurons treated for 21

804 days with either an IgG control (upper panel) or ^{ch}α-GA$_1$ (lower panel). Large irregular

805 extracellular GA$_{50}$-GFP structures were observed only in samples treated with ^{ch}α-GA$_1$

806 antibody (red arrows and bottom right inset). Insets illustrate different GA$_{50}$-GFP

807 intracellular structures observed across all conditions including pre-inclusions (white arrows).

808 Scale = 10 μm and 5 μm. **(C)** Quantification of intracellular GA$_{50}$-GFP structures normalized

809   to the number of nuclei, 36 images per well, 3-6 wells per condition. **(D)** Quantification of

810   GA_{50}-GFP extracellular structures normalized to the number of nuclei, 5 images per well, 3-6

811   wells per condition. Means +/- SD, beta-binomial test. **(E)** Confocal imaging of an $^{ch}\alpha$-GA_1

812   extracellular structure colocalizing with GA_{50}-GFP (upper row), and an IgG control

813   extracellular structure, not colocalizing with GA_{50}-GFP (lower row). Antibodies were

814   detected with α-mouse-Alexa 647. **(F)** Cell viability assay of human neurons expressing

815   GA_{50}-GFP treated with $^{ch}\alpha$-$GA_{1,3}$ or control antibody for 3 days. **(G)** Representative blots of a

816   filter retardation assay where GA_{50}-GFP was detected with an α-GFP antibody. **(H)**

817   Quantification of the filter retardation blot for human neurons treated during 3, 7 or 21 days

818   with $^{ch}\alpha$-GA_1 or IgG control. Intensity of each replicate was normalized to the 3 days IgG

819   control samples. Unpaired t-test is used on the $\log10(x+1)$ transformed data. **(I)** Epi-

820   fluorescent image of GA_{50}-GFP aggregates isolated from transiently transfected HEK293T

821   cells. **(J)** Isolated GA_{50}-GFP aggregates visualized via SEM imaging. **(K)** Representative

822   SEM and corresponding IF images of non-treated (NT) or Alexa Fluor 647-labelled isotype

823   control, α-GA_1- and α-GA_3-treated GA_{50}-GFP aggregates. **(L-M)** Quantification of the

824   surface of the antibody treated GA_{50}-GFP aggregates assessing their porosity **(L)** and the total

825   area of the aggregates **(M)**. NT, n=139; isotype, n=125; α-GA1, n=183; α-GA3, n=193. One-

826   way ANOVA followed by Tukey's multiple comparison test. $P > 0.05$ (no indication), ** $P \leq$

827   0.01, *** $P \leq 0.001$, **** $P \leq 0.0001$.

828   **Fig. 4. Immunoassay with sample denaturation identifies elevated levels of poly-GA in**

829   **brains of mice treated with α-GA antibodies**

830   **(A)** Scheme of chronic antibody treatment in $C9^{450}$ mice receiving intra-peritoneal injection

831   of PBS, $^{ch}\alpha$-GA_1, $^{ch}\alpha$-GA_3, or $^{ch}\alpha$-GP_1 antibodies from 3 to 19 months of age. **(B)** Scheme

832   showing drug-antibody interference in the measurement of poly-GA protein levels using a

833   sandwich-ELISA assay (left panel). Right panel illustrates the effect of sample denaturation

834   prior to measurements. **(C)** Scheme of a mouse brain fractionation protocol adapted to

835   denature samples to avoid interference of the antibody treatment by ELISA. Fractions

836   highlighted in bold were analyzed. **(D, E)** Poly-GA levels measured by immunoassay from

837   the supernatant S1 **(D)** and after ultracentrifugation (supernatant S2 and pellet P2) **(E)** of

838   brains from 7-month-old C9[450]. **(F)** Scheme of chronic antibody treatment by intra-peritoneal

839   injection of $^{ch}\alpha$-GA$_1$ or IgG control to AAV-(G$_4$C$_2$) mice from 2 to 12 months of age. **(G-J)**

840   Poly-GA levels measured by immunoassay from the supernatant S1 **(G, I)** and after

841   ultracentrifugation (supernatant S2 and pellet P2) **(H, J)** of brains from AAV-(G$_4$C$_2$) mice at

842   4 **(G, H)** and 12 **(I, J)** months of age. **(K, L)** Poly-GP levels measured by immunoassay from

843   the supernatant S1 **(K)** and after ultracentrifugation (supernatant S2 and pellet P2) **(L)** of

844   brains from AAV-(G$_4$C$_2$) mice at 12 months of age. Mean ± SD, one-way ANOVA followed

845   by Tukey's multiple comparison tests. Not significant (ns), $P > 0.05$, * $P \leq 0.05$, ** $P \leq 0.01$,
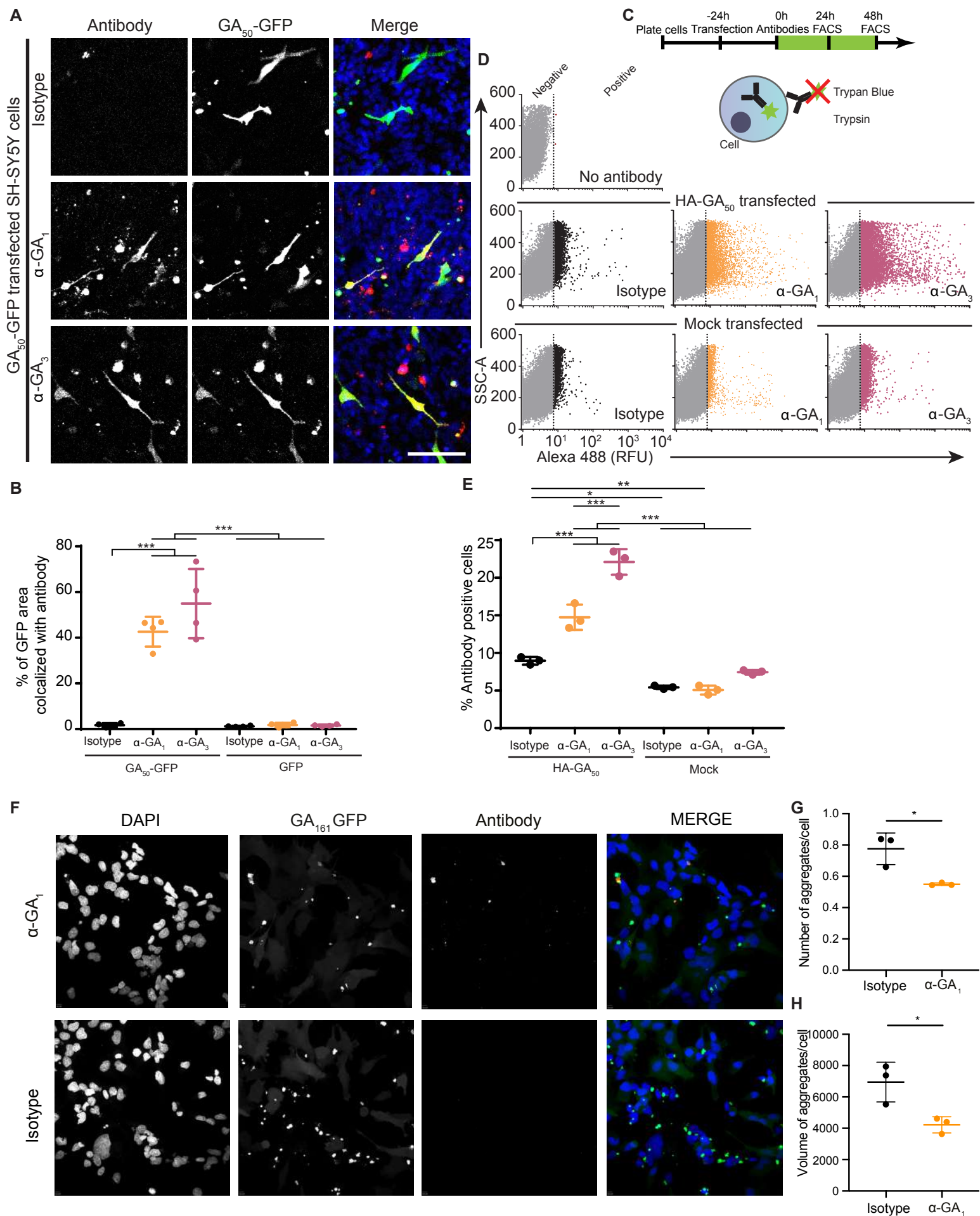
846   *** $P \leq 0.001$.

847   **Fig. 5. Chronic administration of human-derived α-GA$_1$ antibody does not reduce the**

848   **poly-GA and poly-GP aggregate load in brains of AAV(G$_4$C$_2$)$_{149}$ mice.**

849   **(A)** Immunofluorescence of poly-GA staining in the motor cortex (left) and hippocampus

850   (right) of 12-month-old AAV-(G$_4$C$_2$)$_2$ or AAV-(G$_4$C$_2$)$_{149}$ mice treated with $^{ch}\alpha$-GA$_1$ or an IgG

851   control. **(B-C)** Quantifications of percent area occupied by poly-GA aggregates detected with

852   a N-terminal-poly-GA antibody in cortex **(B)** and hippocampus **(C)**. **(D)** Immunofluorescence

853   of poly-GP staining in the motor cortex (left) and hippocampus (right) of 12-month-old

854   AAV-(G$_4$C$_2$) mice treated with $^{ch}\alpha$-GA$_1$ or an IgG control. **(E-F)** Quantifications of percent

855   area occupied by poly-GP staining in cortex **(E)** and hippocampus **(F)**. Scale = 25 μm. Mean

856   ± SD, one-way ANOVA followed by Tukey's multiple comparison test. Not significant (ns),

857    $P > 0.05$, * $P \leq 0.05$.

858 **Fig. 6. Chronic administration of α-GA antibodies impacted only a subset of behavioral**

859 **and neurodegeneration phenotypes in one of two C9ORF72 mouse models**

860 **(A)** Survival Kaplan–Meier curves of C9^{450} and wild-type mice receiving injections of PBS,

861 ^{ch}α-GA$_1$, ^{ch}α-GA$_3$ and ^{ch}α-GP$_1$ antibodies for 16 months. **(B)** Distance traveled in the open-

862 field test by 18-month-old males (n ≥ 8 per group). Mean ± SD, Kruskal-Wallis test followed

863 by Dunnett's multiple comparison tests. **(C)** Nuclei quantification in the hippocampal CA1

864 region in 19-month-old mice (n ≥ 4 mice per group; n ≥ 3 matched sections per mouse).

865 Mean ± SD, one-way ANOVA followed by Dunnett's multiple comparison tests. **(D)**

866 Survival Kaplan–Meier curve of AAV-(G$_4$C$_2$)$_2$ and AAV-(G$_4$C$_2$)$_{149}$ mice receiving injections

867 of ^{ch}α-GA$_1$ or IgG isotype control for 10 months. **(E-G)** Distance traveled **(E)**, velocity of

868 movement **(F)** and time spent moving **(G)** in the open-field test. **(H)** Time taken to fall from

869 inverted grid by 9-month-old AAV-(G$_4$C$_2$) female mice. **(I)** Brain weights of AAV-(G$_4$C$_2$)

870 mice treated for 10 months. Mean ± SD, one-way ANOVA followed by Dunnett's multiple

871 comparison tests. Not significant (ns), P > 0.05, * P ≤ 0.05, ** P ≤ 0.01 and *** P ≤ 0.001.

872

873

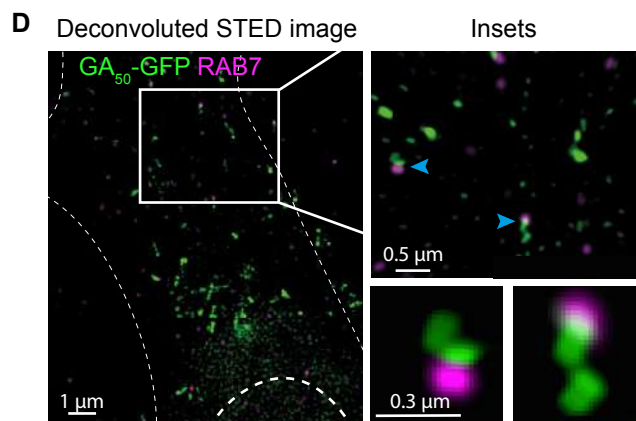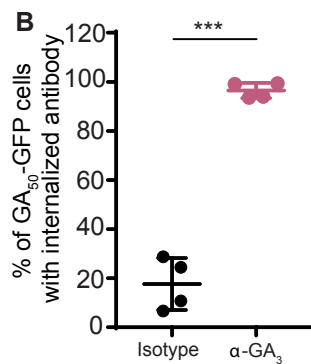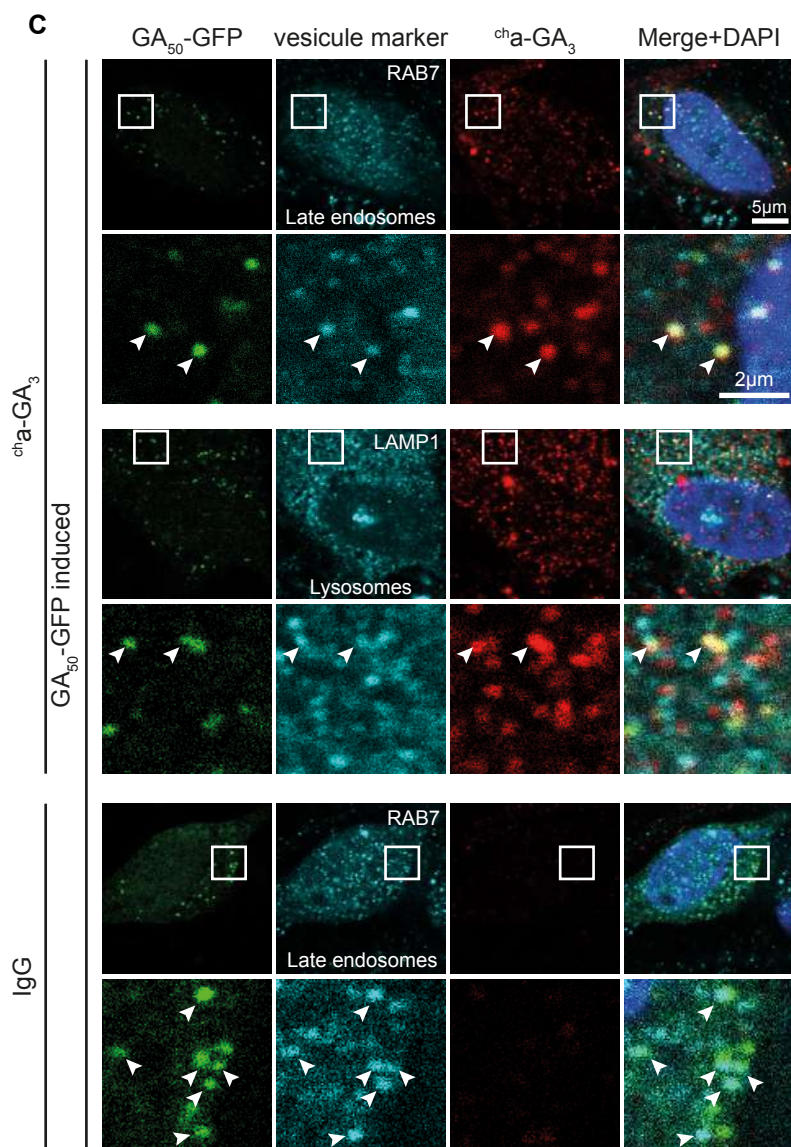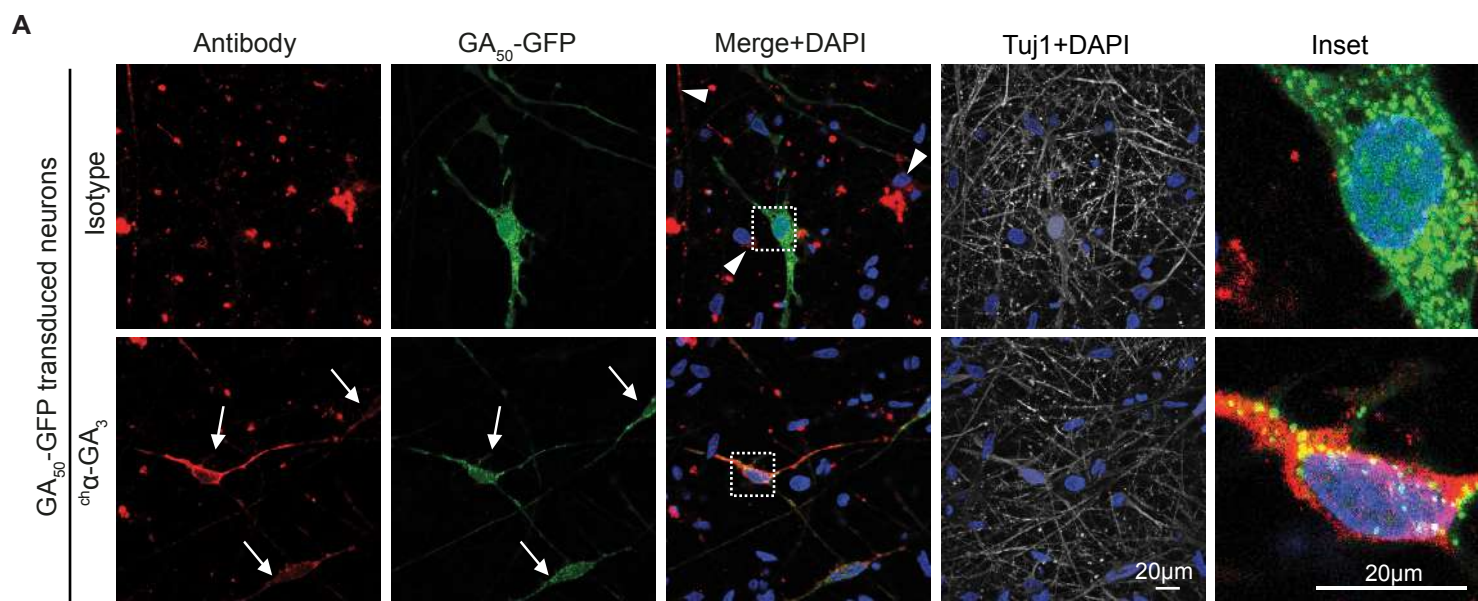Figure 1. Antibody uptake and poly-GA colocalization in living cells
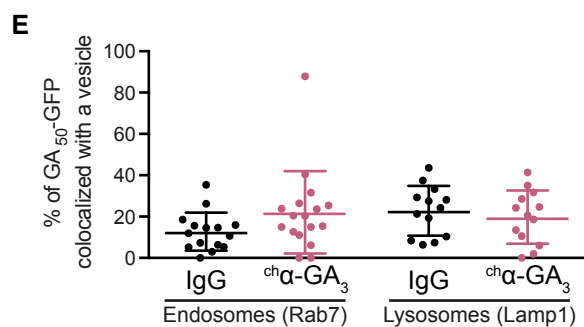
Figure 2. $^{ch}\alpha$-GA$_3$ is internalized via vesicular compartments in human neurons, but does not alter GA$_{50}$-GFP vesicular localization
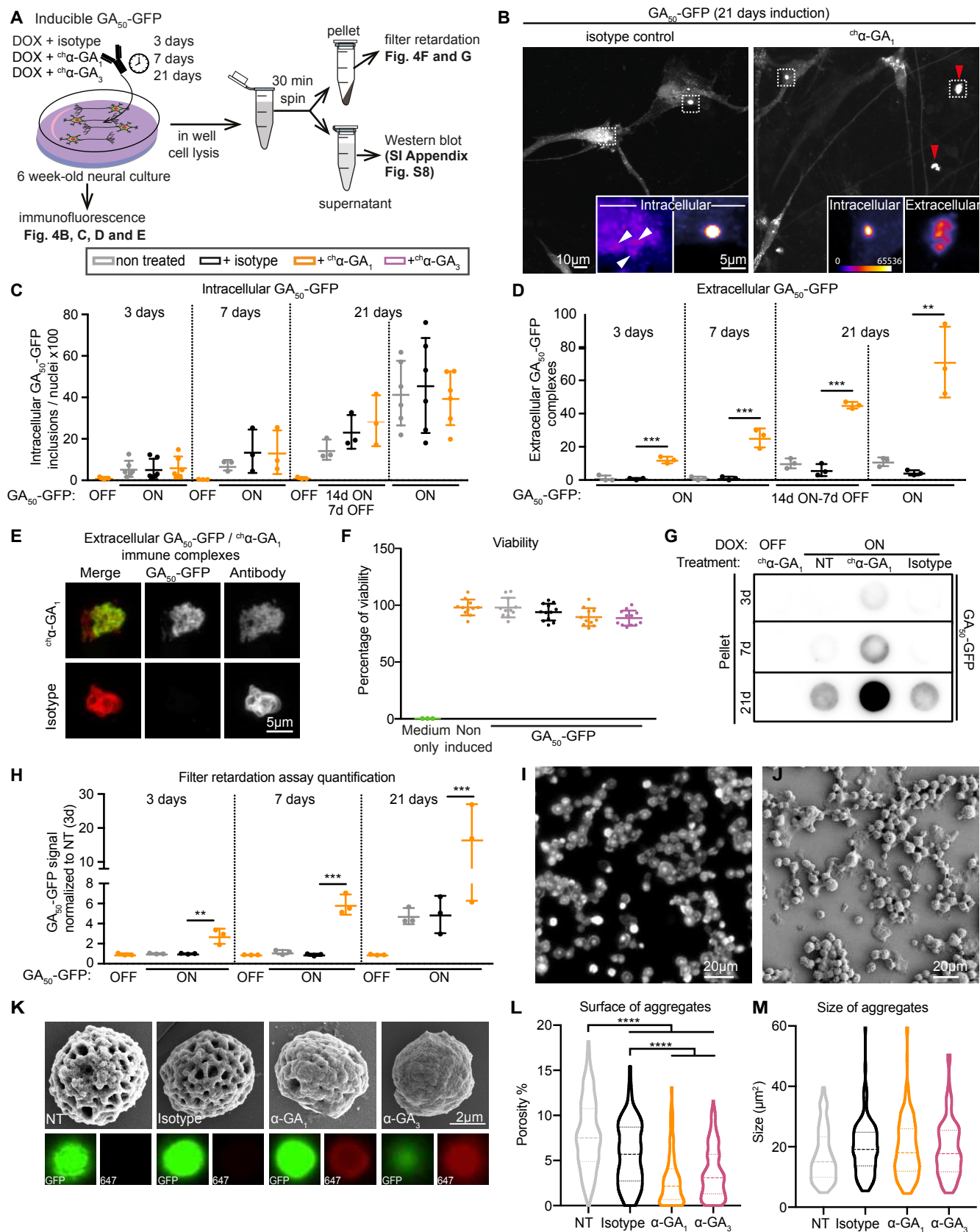
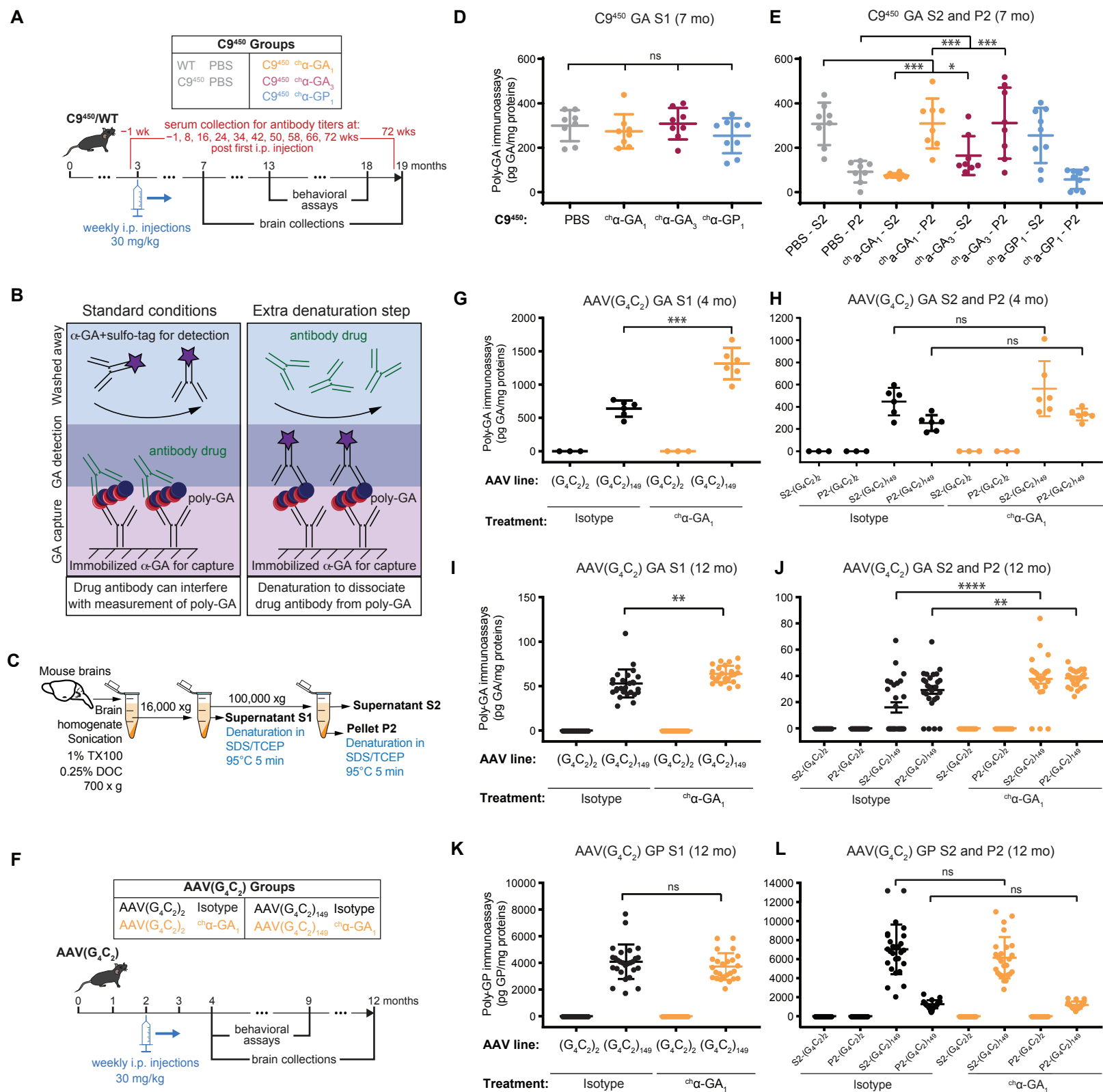Figure 3. Poly-GA and antibodies form large hetero-complexes in long-term treated neuronal cultures

Figure 4. Immunoassay with samples denaturation identifies elevated levels of poly-GA in brains of mice treated with α-GA antibodies
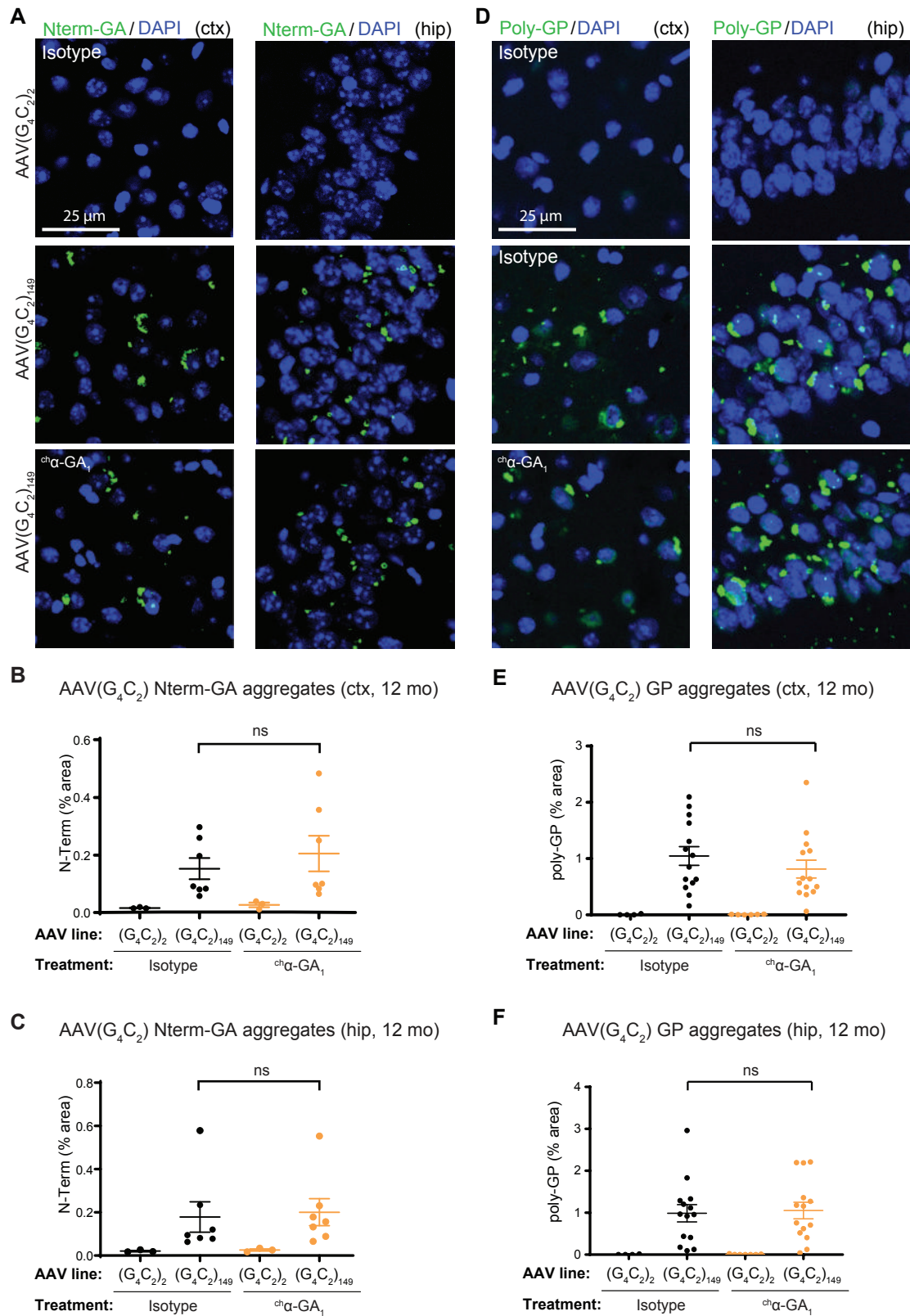
Figure 5. Chronic administration of human-derived α-GA$_1$ antibody does not reduce the poly-GA and poly-GP aggregate load in brains of AAV(G$_4$C$_2$)$_{149}$ mice
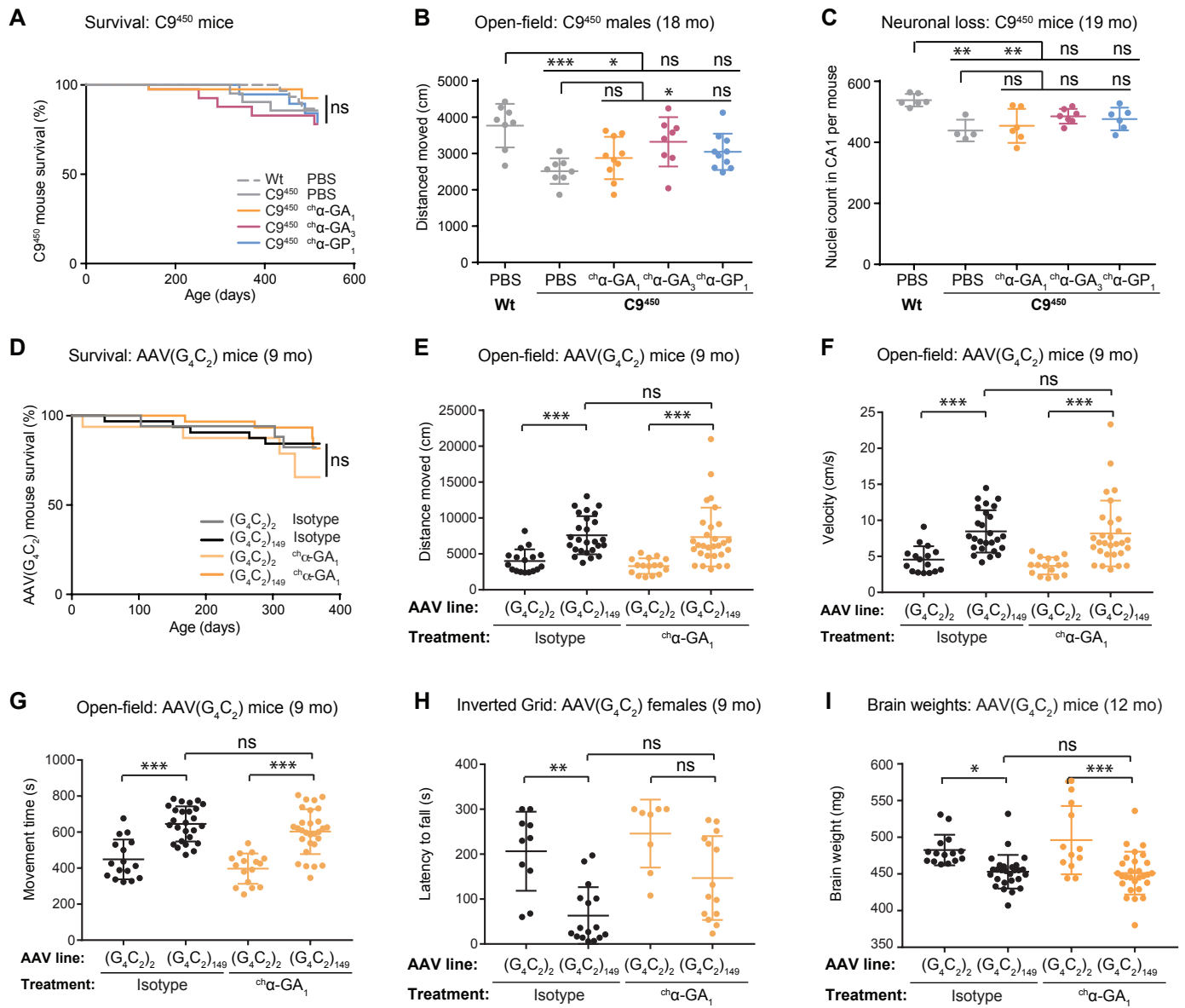
Figure 6. Chronic administration of α-GA antibodies impacted only a subset of behavioral and neurodegeneration phenotypes in one of two C9ORF72 mouse models